Article

Cooling high-density historic districts with strategic greening in the "port-opening area" of Shantou city

Check for updates

Wenqing Liu[1,2] ✉, Junhang Mai[3], Shuang Yuan[1], Haosen Han[1] & Yingzi Wang[1] ✉

This study addresses summer thermal comfort optimization in high-density historic districts, exemplified by the "port-opening area" of Shantou city—an area of renowned for its well-preserved arcade architecture and rich cultural heritage of south east China. Integrating field measurements and ENVI-met simulations, we analyzed how street morphology (orientation, height-to-width ratio) and green infrastructure affect thermal conditions. Results identified peak heat stress (PET > 43 °C) at 14:00–15:00. The 75% tree canopy coverage scheme achieved maximum cooling, reducing PET by 0.45–11.10 °C while generating a Cool Island Spillover Effect that improved adjacent streets. In narrow streets, 2m-high shrubs reduced PET by 0.17– 3.73 °C. Strategic recommendations include deploying decentralized tree greening (50–75% coverage) in open spaces and modular 1–2 m shrubs along pedestrian corridors to synergize shading, ventilation, and heritage preservation. The research provides a data-driven framework for climate-resilient design in heritage-intensive urban contexts.

High-density historic districts, as carriers of urban cultural heritage, are characterized by intensive building layouts, compact spatial textures, and a tight integration of historical architecture with public life[1–3], features that not only preserve the authenticity of traditional urban forms but also pose unique challenges for microclimate regulation[4,5]. In southern China, the traditional "port-opening area" along the inner bay of Shantou City is a typical example of such high-density historic districts (Fig. 1): from the origin of modern markets (1858, with 32 blocks) to the rise of foreign trade and commerce (1983, with 124 blocks), to urban planning during the Republic of China period (1923, with 179 blocks) and its improvement and expansion (1937, with 192 blocks), the number of districts (commercial and residential built-up areas enclosed by roads) and building density here have gradually increased, forming a radial urban road pattern with a building coverage density of up to 41.7%, and making it one of the most prosperous commercial districts along the southern coast of China. Meanwhile, this area is home to China's "arcade building heritage with the largest area and highest density"; most of these buildings were invested and constructed by overseas Chinese returning to China, and are regarded as the spiritual homeland of the Chaoshan people.

In recent years, with the rise of tourism in Chaoshan's overseas Chinese hometowns and the exploration of the heritage value of the arcade buildings, the port-opening area of Shantou has become one of the most culturally vibrant and economically promising historic districts in the southeast

coastal region[6–8]. Meanwhile, against the backdrop of a surge in tourist numbers and the intensified urban heat island (UHI) effect driven by urbanization, the worsening trend of the summer microclimate in this area, especially the deterioration of thermal comfort, has become increasingly prominent[9–11], and this has evolved into a key factor restricting the experience of external tourists to the heritage site and the outdoor activities of local residents. The worsening summertime thermal stress has directly led to diminished visitor experience and restricted outdoor activities for residents, which not only threatens the social vitality of the district but also poses potential risks of thermal fatigue damage to the historic buildings due to frequent extreme heat. Currently, how to alleviate the contradiction between the sustainable development of this historic district and the hot outdoor climate in summer has become a practical issue that must be addressed.

In the context of aggravated climate change, the optimization of thermal comfort in outdoor spaces of historic districts has attracted widespread attention. Existing achievements mainly focus on two aspects: one is to explore the influencing factors and indicators of regional thermal comfort; the other is to propose and assess improvement strategies, and apply them to urban renewal design.

The first aspect of research primarily focuses on climate parameters, ground materials, and building layouts. For instance, Jamei[12] evaluated outdoor thermal comfort in the historical district, new district, and suburbs of a historical town using the heat intensity index and relative humidity

[1]Department of Civil Engineering and Intelligent Construction, College of Engineering, Laboratory of vernacular architecture Surveying and Mapping, Shantou University, Shantou, China. [2]Laboratory for Digital-Intelligent Design of Cultural Heritage, Shantou University, Shantou, China. [3]School of Architecture, South China University of Technology, Guangzhou, China. ✉e-mail: wqliu@stu.edu.cn; yzwang@stu.edu.cn
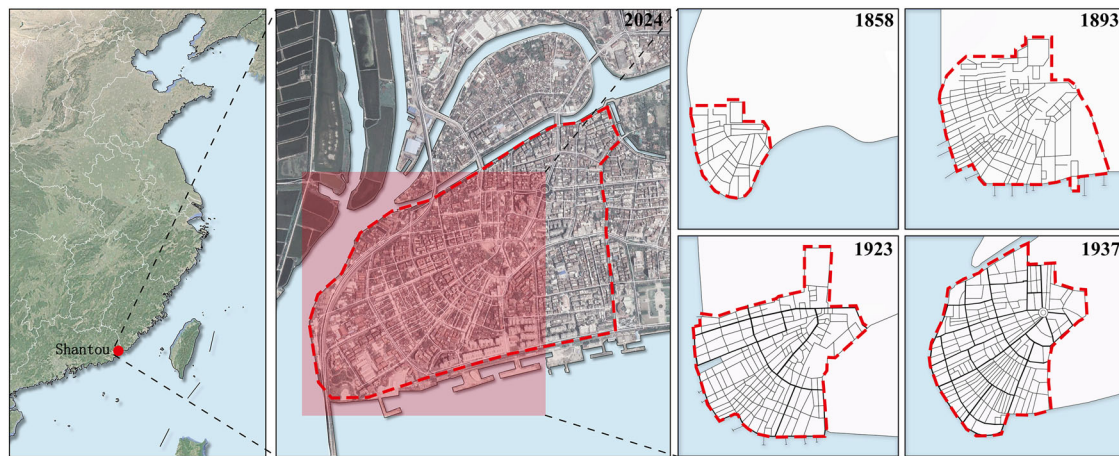
Fig. 1 | The location and evolution of the urban fabric of "port-opening area" of Shantou city. Red circle indicates the location of Shantou City; Red rectangle indicates the location of "port-opening area"; Red dashed lines indicate the changes in the scale of "port-opening area".

(RH)[12]. Chu et al.[13] analyzed the impact of natural ventilation on outdoor thermal comfort in historical districts, where historical buildings and new constructions are mixed, and proposed planning and layout recommendations for new buildings[13]. Ragheb et al.[14] highlighted that air temperature (AT), RH, airflow, and solar radiation (SR) in historical districts significantly influence human thermal comfort[14]. Castaldo[15] investigated the effects of vegetation, surface materials, and building density in mountainous city historical districts on pedestrian comfort[15]. Biqaraz et al.[16] identified the lack of greenery coverage in public spaces as a key factor contributing to residents' dissatisfaction with outdoor thermal environments in historical districts[16]. Bochenek et al.[17] studied the impact of street tree forms on human thermal comfort through a historical district renewal project[17]. Yang et al.[18] combined microclimate measurements, surveys, and simulations to explore thermal comfort evaluation indicators and thresholds for Beijing's historical districts[18].

The first research stream investigates the influence of climate parameters, ground materials, and building layouts on the thermal environment of historic districts. Studies in this area have employed tools such as the heat intensity index to evaluate outdoor thermal comfort across varied urban settings, including historic cores, newer developments, and suburban zones[12]. In contexts where historic and contemporary buildings coexist, research has emphasized the role of natural ventilation in shaping thermal comfort, offering planning and design guidance for new constructions[13]. Key microclimatic elements, such as AT, humidity, airflow, and SR, have been identified as critical factors in historical urban settings[14]. Further work has explored how vegetation, surface materials, and building density jointly affect pedestrian thermal perception, particularly in mountainous city contexts[15]. The significance of greenery is further underscored by studies linking insufficient vegetation in public spaces to resident dissatisfaction with thermal conditions[16]. Morphological attributes of street trees have also been examined through regeneration projects, revealing their nuanced role in modifying human thermal comfort[17]. Complementing these focused inquiries, integrated methodologies combining microclimate measurements, surveys, and simulation have been applied to establish evaluation frameworks and thermal comfort thresholds in Beijing's historic districts[18]. Extending these insights, research in high-density urban environments confirms that tree coverage must reach a critical threshold to produce meaningful cooling benefits[19]. This is supported by Beijing Dashilar–based analyses identifying three-dimensional green volume as the principal predictor of thermal comfort, with densely vegetated zones exhibiting markedly lower PET values[20]. In parallel, studies addressing high-density urban constraints propose integrated strategies, including site-specific planting and systematic maintenance, to embed trees within tightly built environments[21].

The second research direction centers on the application of integrated improvement strategies to enhance outdoor thermal comfort in high-density historical neighborhoods. These include the use of high-reflectance pavement materials to mitigate thermal stress in street canyons[22], the design of shading structures informed by passive cooling principles in hot-arid climates[23], and the strategic incorporation of street trees, whose microclimate benefits have been quantitatively confirmed through field measurements and simulations[24]. Recent studies further address the specific thermal comfort needs of vulnerable groups such as the elderly, promoting context-aware renewal strategies in historic settings[25]. Urban renewal case studies additionally highlight the challenge of reconciling thermal performance with broader livability objectives[26]. Beyond conventional approaches, emerging studies explore vertical greening systems, indicating that substantial facade coverage can yield measurable temperature reductions in compact urban forms[27]. Coupled simulation studies further refine vegetation planning by quantifying the trade-offs between cooling energy savings and humidity increases under different greening configurations[28]. At the neighborhood scale, optimized spatial arrangements of trees, particularly in sun-exposed areas, have been shown to enhance cooling efficiency[29], while centralized greening layouts that employ continuous and enclosed planting have been proposed to extend the spatial reach of thermal comfort improvements[30].

The main indicators for assessing outdoor thermal comfort include the physiological equivalent temperature (PET), standard effective temperature (SET), and universal thermal climate index (UTCI)[31,32]. Among these, PET integrates environmental parameters such as AT, RH, WS, and SR, and additionally incorporates individual physiological factors such as human metabolic rate and clothing thermal resistance. This makes PET capable of more comprehensively reflecting the differences in human thermal perception, making it one of the most frequently used thermal comfort evaluation indicators[33,34]. In this study, PET is selected as the primary indicator for thermal comfort evaluation.

In summary, the thermal comfort level of outdoor spaces in historic districts is a result of the combined effects of four microclimate factors: AT, RH, wind speed (WS), and SR. Individual climate indicators alone cannot fully reveal human outdoor thermal sensations, and the dominant factors influencing thermal comfort vary among different space configurations[35,36]. Additionally, human perception of the spatial environment also influences thermal comfort[37,38], and optimization measures in urban thermal environment research have become increasingly diversified, with a growing focus on human experience[39–42]. Improvements through landscaping, especially greening strategies, are considered more natural, environmentally friendly, and aligned with human physiological sensations, thus receiving increasing attention[43–45].

Fig. 2 | Plan of the study area. Red rectangle indicates the study area; Red dashed line indicates the boundary of "port-opening area".

The Existing research on outdoor thermal comfort optimization in historic districts focuses on influencing factors or single improvement strategies, but lacks comprehensive exploration of the synergistic effects of greening type, layout, and coverage, especially in high-density historic districts. It also rarely integrates historic district constraints (heritage view protection, pedestrian flow) or quantifies the "Cool Island Spillover Effect" of greening. A gap remains in matching greening configurations to different spaces of high-density historic districts while balancing heritage conservation and thermal comfort.

This study takes the high-density historic district in Shantou's port-opening area, characterized by well-preserved arcades, as research object. By integrating field microclimate measurements and ENVI-met simulations, it aims to clarify the distribution of microclimate and thermal comfort (evaluated by the PET index) during the summer peak heat period (14:00–15:00), analyze the interactive effects between street morphology and green infrastructure, design context-adapted greening schemes for the district, quantify the effects of these schemes, and ultimately propose a greening strategy framework.

Building on this, we propose two research questions: (1) How to use field measurements and ENVI-met simulations to capture summer microclimate/thermal comfort distribution in the study area and identify key influencing factors? (2) How to design greening schemes balancing heritage conservation/pedestrian needs, and quantify their thermal comfort optimization effects?

Addressing these questions fills the gap in integrated greening research for high-density historic districts, provides a targeted technical framework for thermal comfort optimization, and promotes the integration of heritage conservation and climate resilience in urban renewal.

Methods
Study area and data source
Research on urban microclimate mainly focuses on small and medium scales, as the deterministic processes of meteorological conditions are more prominent at this scale[46]. As shown in Fig. 2, this study focuses on a suitable-scale area of 230×270 m², which centers on Zhongshan Pavilion—a landmark building in the Shantou Port Opening Area. With the pavilion as the starting point, a central square is formed by radiating outward, and this square is connected to five surrounding radial pedestrian streets, constituting the most densely populated and built-up historical block in Shantou city.

This study uses three main data sources. First, on-site mapping provides data on street/building forms and scales for the site survey phase. As Table 1 shows, since the 2010s, street-facing building facades in the study area have been renovated, with original facade decorations and street spaces restored and cleaned; following this, we remeasured street widths and building heights on both sides via laser rangefinder. Measurements show: Guoping Road (north-south) is 10 m wide, with average building height of 15 m and H/D ratio of 1.5; Shengping Road (east-west) is also 10 m wide, with average adjacent building height of 11 m and H/D ratio of 1.1; Yuanqian Road (northern part) is approximately10m wide, with average building height of 12 m and H/D ratio of 1.2.

Second, the microclimate status data required for the current situation assessment phase are mainly obtained from meteorological stations and on-site monitoring. Specifically, this is accomplished by collating the 10-year meteorological data (2011–2020) from the Shantou Meteorological Station (Station Number: 59316) and combining it with on-site monitoring data from microclimate measuring equipment. Third, the microclimate index data and thermal comfort data required for the optimization simulation phase are mainly derived from computational fluid dynamics (CFD) simulations, with specific operations carried out using the ENVI-met software.

Field measurement of microclimate
Using daily meteorological data from Shantou Weather Station (Station Number: 59316, 2011–2020), we conducted monthly temperature statistics. The average maximum temperatures for June, July, and August over the past decade are 31.96 °C, 33.14 °C, and 32.99 °C, respectively, with 70% of summer daily maximum temperatures falling between 31 °C and 34.4 °C. Focusing on summer, we selected June 20th (temperature: 32.6 °C) as the measurement date, aligning with the mid-value of Shantou's summer high-temperature frequency range, to ensure representative street thermal comfort data. Measurements were taken from 9:00 a.m. to 7:00 p.m. (10 h of continuous monitoring), covering the peak pedestrian period in the historical district, with parameters including RH, AT, and WS.

Four observation points with uniform ground conditions were selected (Fig. 3) to isolate the impacts of street orientation and spatial openness on microclimate: Point 1 (southeast-oriented Guoping Road), Point 2 (east-west-oriented Shengping Road), Point 3 (intersection of north-south Guoping Road and east-west Yuanqian Road), and Point 4 (central square).

As shown in Fig. 4a, hourly AT at all points (9:00–19:00) follows a similar trend: rising from 9:00, peaking at 14:00, then declining, with the highest AT recorded between 13:00 and 15:00. Point 4 had the highest AT (likely due to unobstructed SR on the square's large paved area), while Point 1 had the lowest, with a maximum AT 2.3 °C lower than Point 4, possibly because the southeast-oriented street's higher aspect ratio reduces SR. Points 2 and 4 had relatively consistent AT, indicating east-west Shengping Road is more affected by SR; Point 3's AT was 1.1 °C lower than Point 4 on average (13:00–16:00), suggesting more open spaces are more susceptible to SR. As shown in Fig. 4b, hourly RH at all points shows no significant differences, with a trend inversely correlated to AT (declining to a minimum at 14:00);

Table 1 | Building facades along streets in the study area

Position	Facade along the street
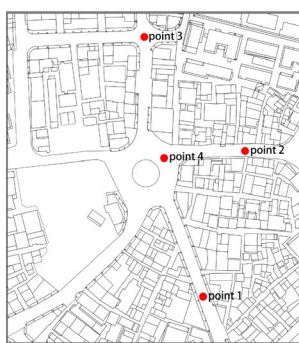
a. Measuring point locations   b. Point 1   c. Point 2   d. Point 3   e. Point 4

Fig. 3 | locations of 4 measured points. a Measuring point locations; **b** Point 1; **c** Point 2; **d** Point 3; **e** Point 4. Red circle indicates the location of measuring point.

Point 2 had the lowest RH (42.1%). As shown in Fig. 4c, analysis of hourly average WS reveals Point 1 had the lowest WS (max: 1.35 m/s), while Point 4 had stable, gradually increasing WS (attributed to the square's open layout improving air circulation). Point 2's hourly average WS was slightly higher than Point 4 (likely due to airflow from the square compressing air density on Shengping Road), and Point 3's WS fluctuated significantly (12:00–14:00), possibly from local airflow variations.

With the straight-line distance between observation points ≤300 meters, and under consistent natural climatic conditions and paving materials, street orientation and spatial openness are inferred as key factors driving microclimate differences. From AT, RH, and WS data: Point 3 (narrow intersection) had significantly lower average WS than Point 4 (open square), and notably lower AT (13:00–15:00)—suggesting WS is primarily influenced by spatial openness, while AT is dominated by SR. Additionally,
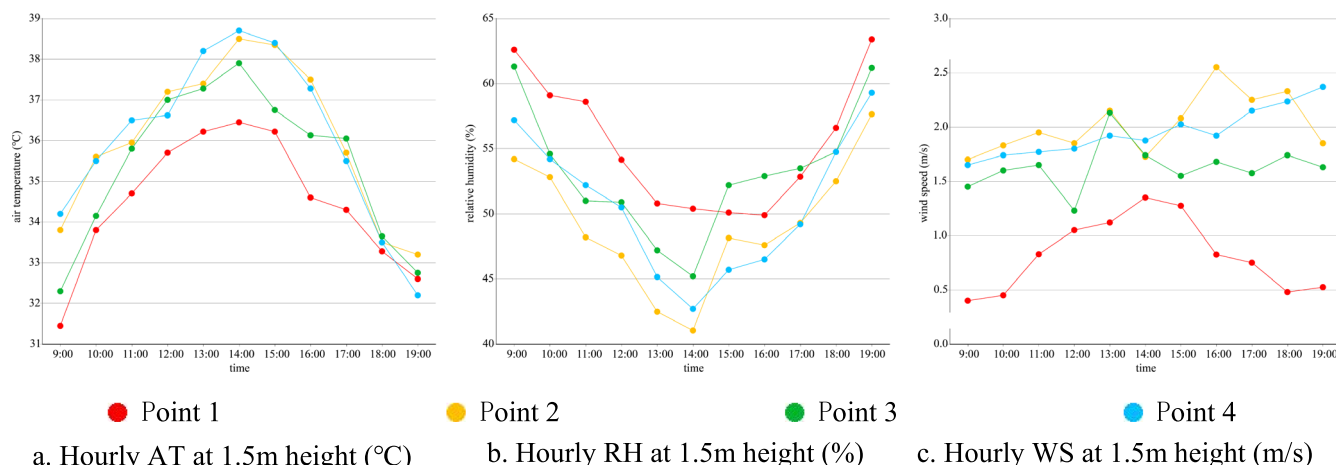
a. Hourly AT at 1.5m height (°C)　　b. Hourly RH at 1.5m height (%)　　c. Hourly WS at 1.5m height (m/s)

Fig. 4 | Hourly air temperature measurements at four points. a Hourly AT at 1.5 m height (°C); **b** Hourly RH at 1.5 m height (%); **c** Hourly WS at 1.5 m height (m/s). Red point indicates point 1; Orange point indicates point 2; Green point indicates point 3; Blue point indicates point 4.

Table 2 | Initial parameter settings for simulation model

Type	Parameter information	
Base location	Shantou port district	23°32′N, 116°45′E
	Roughness of near-surface	0.1
simulation time	Starting time	8:00 on June 20, 2021
	Simulation duration (h)	11
	Wind direction (°)	260
Meteorological parameters	Continuous wind speed (m/s)	2.09
	cloud cover	0
Underlying surface material	Asphalt/soil/permeable pavement	Default values in ENVI-met
Horizontal boundary condition	-	Forced

Point 1 (southeast Guoping Road, H/D = 1.5) had lower average WS and AT (13:00–15:00) than Point 2 (east-west Shengping Road, H/D = 0.9), indicating street orientation and H/D strongly affect SR. Since point measurements cannot represent the entire street's microclimate, simulations will further explore how street orientation, H/D, and other spatial features influence microclimate.

Microclimate simulation

A 230 × 270 m² block model (max building height: 24 m) was constructed in ENVI-met. To enhance accuracy, five blank grids and ten nested grids were added around the simulation area; horizontal grids (240 × 280) had a 1 × 1 m² resolution, and vertical grids (27 total) used an elastic system with a 10% amplification factor above 5 m. Four receptor points were set to match the field observation points, with simulation details (date, location, underlying surface materials) outlined in Table 2. Hourly AT and RH inputs were sourced from real-time data at Shantou Weather Station (Station Number: 59316, Fig. 6), and the simulation ran from 8:00 to 19:00.

As shown in Figs. 5 and 6, measured and simulated AT/RH (1.5 m above ground) were compared: all points' measured and simulated AT peaked at 14:00, with near-identical maximum AT for Points 1 and 3. Simulated AT for Points 1, 3, and 4 were slightly lower than measured values (9:00–14:00), while Point 2's measured and simulated AT showed high consistency. RH variation trends were generally similar, with measured values fluctuating more and simulated values remaining smoother.

The errors between the measured and simulated values were calculated using the RMSE and MAPE indicators. As shown in Table 3, the RMSE values for AT range from 0.42 to 0.96 °C, and the MAPE values range from 0.95 to 2.24%. For RH, the RMSE values range from 2.68 to 3.24%, and the MAPE values range from 4.13 to 4.92%. The RMSE values for AT at all measurement points are below 1.63 °C, and the RMSE values for RH are below 5%, with MAPE values below 10%. All measurement points are within the allowable error range, indicating that the simulation results can effectively analyze and predict the microclimate environment of the study area.

Results

The assessment of current microclimate and thermal comfort

Air temperature and radiation. Based on field measurements and simulation analysis, the period from 13:00 to 15:00 is the time when the daytime temperature reaches its peak within the study area. This period has been selected for analysis. Building shadows dynamically regulate the reception and conversion of SR, forming a thermodynamic equilibrium system with temperature, where the interactions among these elements play a crucial role in controlling thermal comfort[47–49]. As shown in Fig. 7 and Fig. 8, the meteorological data, including AT, direct SR (DSR), diffuse radiation (DR), and reflected radiation (RR), calculated by ENVI-met software, are visualized in the Leonardo module.

Between 13:00 and 15:00, the change in solar altitude angle causes the area of building shadows to gradually increase, effectively blocking SR. The radiation values of DSR range from 929.34 to 1003.66 W/m², while the radiation values of DR during this period range from 1.25 to 120.25 W/m², and the radiation values of RR range from 252.8 to 401.46 W/m². During this period, the impact of DSR on AT is greater than that of RR, which in turn has a greater impact than DR.

During the same period, Guoping Road exhibits the highest RR but the lowest AT. This phenomenon may be attributed to Guoping Road having the largest building shadow area, where shading effectively reduces AT. At 14:00, the AT reaches its peak within the study area, with AT ranging from 35.18 to 37.02 °C. Under identical conditions of time and paving materials (with varying shaded area distributions), AT variations along the same street are primarily influenced by differences in DR, RR caused by shaded area differences. When direct SR is constant, the RR values of the square, the vacant land, and the western section of Shengping Road vary with the albedos of different underlying surfaces. However, the AT over the vacant land, which has a soil substrate, is lower than that over the permeable pavement of the square. The AT difference at 13:00 is 0.7 °C, at 14:00 is 0.6 °C, and at 15:00 is 0.7 °C, with an average difference of 0.67 °C during the high-temperature period. Similarly, the AT over the asphalt pavement on the eastern section of Shengping Road is higher than that over the permeable
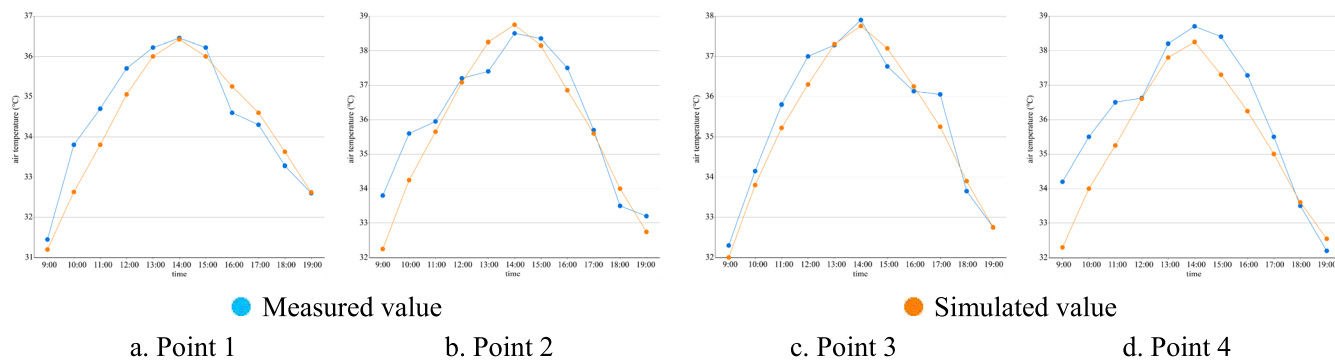
Measured value   Simulated value

a. Point 1   b. Point 2   c. Point 3   d. Point 4

Fig. 5 | Comparison of measured and simulated air temperature values. a Point 1; **b** Point 2; **c** Point 3; **d** Point 4. Blue point indicates measured value; Orange point indicates simulated value.

Measured value   Simulated value

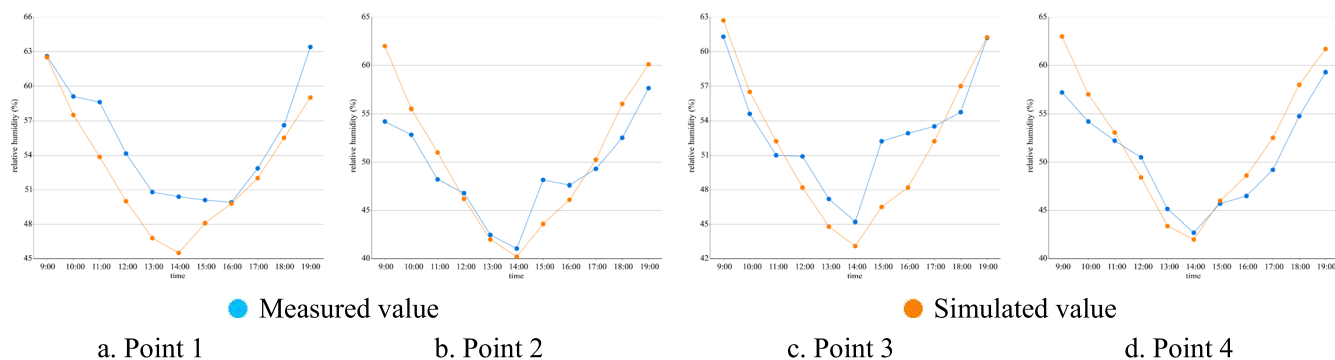a. Point 1   b. Point 2   c. Point 3   d. Point 4

Fig. 6 | Comparison of measured and simulated values of relative humidity. a Point 1; **b** Point 2; **c** Point 3; **d** Point 4. Blue point indicates measured value; Orange point indicates simulated value.

Table 3 | Analysis of RMSE and MAPE between measured and simulated values at 1.5 m

Measure point	Air temperature		Relative humidity	
	RMSE (°C)	MAPE (%)	RMSE (%)	MAPE (%)
Point 1	0.59	1.34	3.08	4.92
Point 2	0.74	1.65	3.24	4.76
Point 3	0.42	0.95	2.73	4.65
Point 4	0.96	2.24	2.68	4.13

pavement on the western section. The AT difference at 13:00 is 1.2 °C, at 14:00 is 0.9 °C, and at 15:00 is 1.1 °C, with an average difference of 1.07 °C during the high-temperature period. The comparison results indicate that the impact of the three paving materials on AT within the study area is ranked as follows: asphalt > permeable pavement > soil.

Under the same street orientation at the same time, Yuanqian Road, with a H/D ratio of approximately 1.2, has a larger building shadow area compared to the eastern section of Shengping Road, which has a H/D ratio of approximately 0.9. This suggests that, during the summer high-temperature period, streets with a higher H/D ratio within the study area are more effective in blocking SR and thus better at reducing AT.

Relative humidity and wind speed. As depicted in Fig. 9, during the timeframe of 13:00 to 15:00, the overall trend of changes in RH at various moments is inverse to that of AT, with RH decreasing as AT rises. At 14:00, notable temperature variations are observed among Guoping Road, Shengping Road, and Yuanqian Road, whereas there is little variation in RH. Under peak AT conditions, the RH at 14:00 has nearly reached its lowest point of 45.31%. Simultaneously, although the AT in

the unused space on the west side of the Central square is not the lowest within the study area, the RH there is generally higher than in other districts. This could be attributed to the natural soil underlying this area, as the evaporation of soil moisture elevates the RH. Furthermore, despite no significant fluctuations in WS across different time periods within the same region, the changes in RH are pronounced, indicating that, during this period, RH within the study area is more prominently influenced by AT.

As shown in Fig. 10, during the 13:00–15:00 period, the overall WS varies within the range of 0–2.71 m/s. In some areas of the west side of the central square, WS slightly increases, while WS in other spaces shows no significant changes. At the same moment, WS differences are significant across different regions. The maximum WS in the central square can reach 2.43 m/s, and in the unobstructed area near Shengping Road (within the vacant space on the west side), the WS can reach as high as 2.59 m/s. In the semi-enclosed area near Anping Road, the WS is relatively low, with a minimum of only 0.09 m/s. The WS on Shengping Road and Yuanqian Road, which run east-west, are notably higher than those on Guoping Road. Additionally, the WS in the eastern section of Shengping Road and some areas of Yuanqian Road show significant variations, which may be due to the canyon effect caused by the alignment between the east-west orientation of the streets and the wind direction on the simulation day.

Thermal comfort. We imported the atmosphere data output by ENVI-met into the BIO-met module, and calculated the PET thermal comfort index by using summer clothing thermal resistance and a metabolic rate of 86.21 W/m². The thermal comfort scale of PET can be divided into nine levels: very cold, cold, cool, slightly cool, neutral, slightly warm, warm, hot, and very hot[50], with each level corresponding to a PET temperature range from low to high. The neutral range refers to the PET value range when the human body subjectively feels comfortable. Due to the
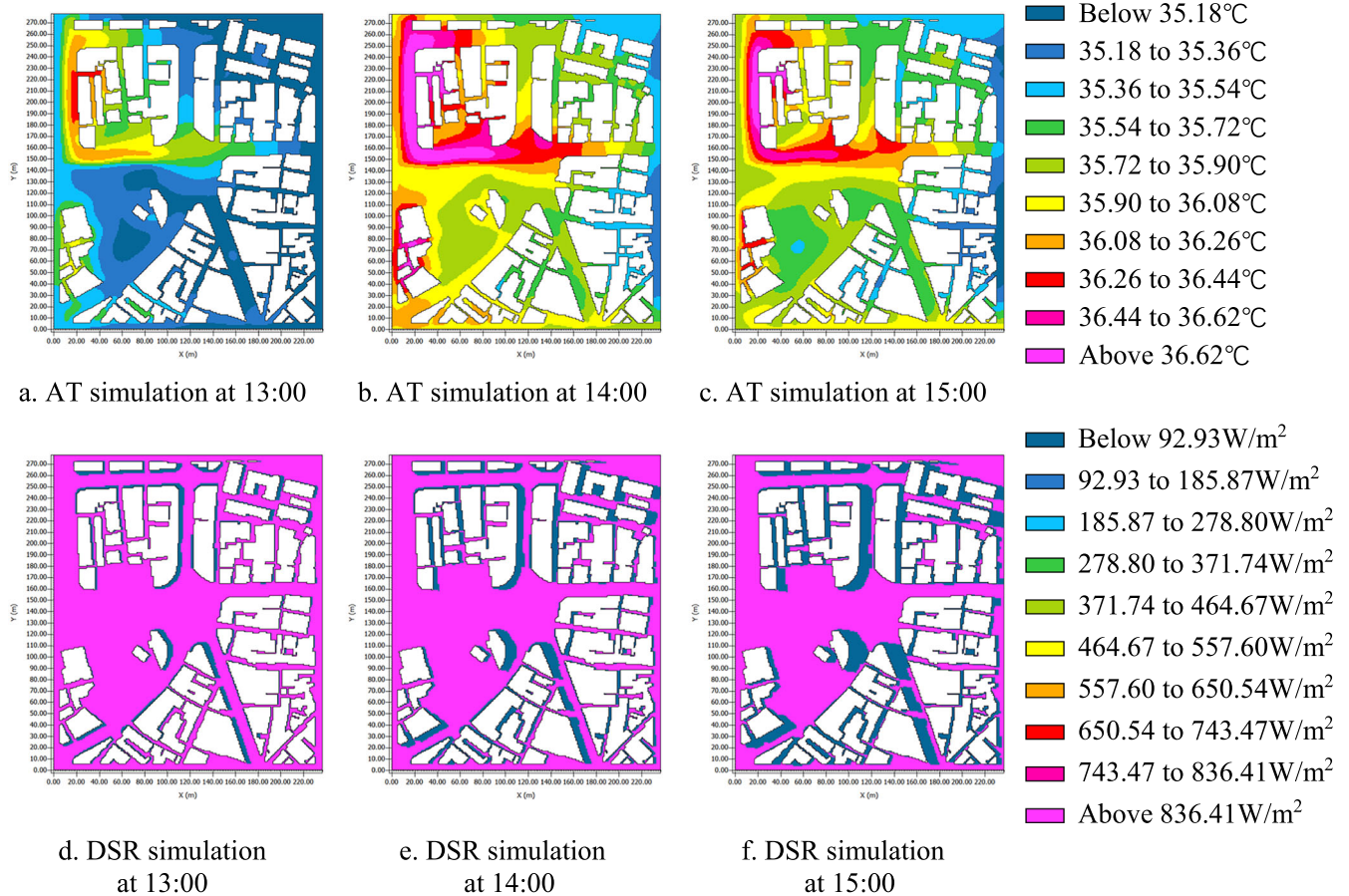
Below 35.18℃	
35.18 to 35.36℃	
35.36 to 35.54℃	
35.54 to 35.72℃	
35.72 to 35.90℃	
35.90 to 36.08℃	
36.08 to 36.26℃	
36.26 to 36.44℃	
36.44 to 36.62℃	
Above 36.62℃	

a. AT simulation at 13:00   b. AT simulation at 14:00   c. AT simulation at 15:00

Below 92.93W/m^2	
92.93 to 185.87W/m^2	
185.87 to 278.80W/m^2	
278.80 to 371.74W/m^2	
371.74 to 464.67W/m^2	
464.67 to 557.60W/m^2	
557.60 to 650.54W/m^2	
650.54 to 743.47W/m^2	
743.47 to 836.41W/m^2	
Above 836.41W/m^2	

d. DSR simulation at 13:00   e. DSR simulation at 14:00   f. DSR simulation at 15:00

Fig. 7 | Simulated AT and DSR from 13:00 to 15:00. a AT simulation at 13:00; **b** AT simulation at 14:00; **c** AT simulation at 15:00; **d** DSR simulation at 13:00; **e** DSR simulation at 14:00; **f** DSR simulation at 15:00. AT air temperature, DSR direct solar radiation.

influence of various factors such as climate environment and social culture on thermal comfort evaluation, the thermal comfort evaluation criteria need to be adjusted according to the local PET neutral range. Based on the PET grading standards of regions with similar climate environments such as Hong Kong, Taiwan, and Guangzhou[50–53], it is known that the summer neutral PET index range in Shantou City is between 21 and 29 °C.

As shown in Fig. 11, the maximum PET values at all measurement points occur during the 14:00 and 15:00 periods, which is the worst time for thermal comfort during the day. As shown in Fig. 13, by visualizing the 14:00 and 15:00 data in the Leonardo module, it can be seen that the PET high-temperature area distribution is the largest within the street space at 14:00. During the high-temperature period, the PET values within the study area are all above 43 ℃, and this period falls under the "very hot" level. The five pedestrian streets face thermal environment safety hazards and are unsuitable for visitors to tour.

As shown in Fig. 12, for east-west oriented streets, the PET values on both sides of Yuanqian Road are lower than those on the east side of Shengping Road, which has the same orientation. The areas with relatively lower PET values coincide with the shaded areas. For north-south oriented streets, Guoping Road exhibits different PET values divided by building shadows, with the northern section having better thermal comfort than the southeast section. On Anping Road (runs from southeast to northwest), sections without building shading even have PET values exceeding 52.40 ℃. The western side of the central square and the east side of Shengping Road have relatively lower PET values. Combining these PET area distribution observations with microclimate simulation results, it is found that areas with lower PET values coincide with areas of higher WS. During this period, the AT on the east section of Shengping Road is higher than that on the

southeast section of Guoping Road, with the same RH. However, due to the higher WS on the east section of Shengping Road, its PET value is significantly lower than that of the southeast section of Guoping Road. This suggests that at 14:00 and 15:00, direct sunlight and WS have a more significant impact on thermal comfort within the study area.

Comparing the simulation results, it is evident that the time of highest temperature coincides with the time of poorest thermal comfort, but their spatial distributions are not entirely consistent. This is because the PET thermal comfort index is influenced by multiple factors, including AT, RH, WS, and mean radiant temperature. Comparison of mean radiant temperature and wind speed shows that spaces with higher mean radiant temperature and lower WS within the study area have higher PET values and poorer thermal comfort. Examples include Guoping Road, Anping Road, and the unused area west of the square near Anping Road.

The assessment of PET optimization from greening schemes

Open space: As shown in Fig. 13, in the vacant land area west of the central square, three different greening schemes were created by selecting tree coverage rates of 25%, 50%, and 75%, while maintaining a consistent ground cover coverage rate of 80%. The thermal comfort of these schemes was then compared through simulation results.

In terms of site plan design, we positioned the site entrances and exits according to the pedestrian flow direction in the study area. The entrance on the northeast and southeast sides facilitate visitors' access and linger, while the entrances on the northwest and west sides are convenient for residents. Additionally, the layout follows the road fabric on the west and southeast sides, forming a radial road network to enhance accessibility for visitors. Furthermore, to minimize visual impact on visitors in the historic district and to screen the parking lot to the north, we adopted a dispersed, aligned
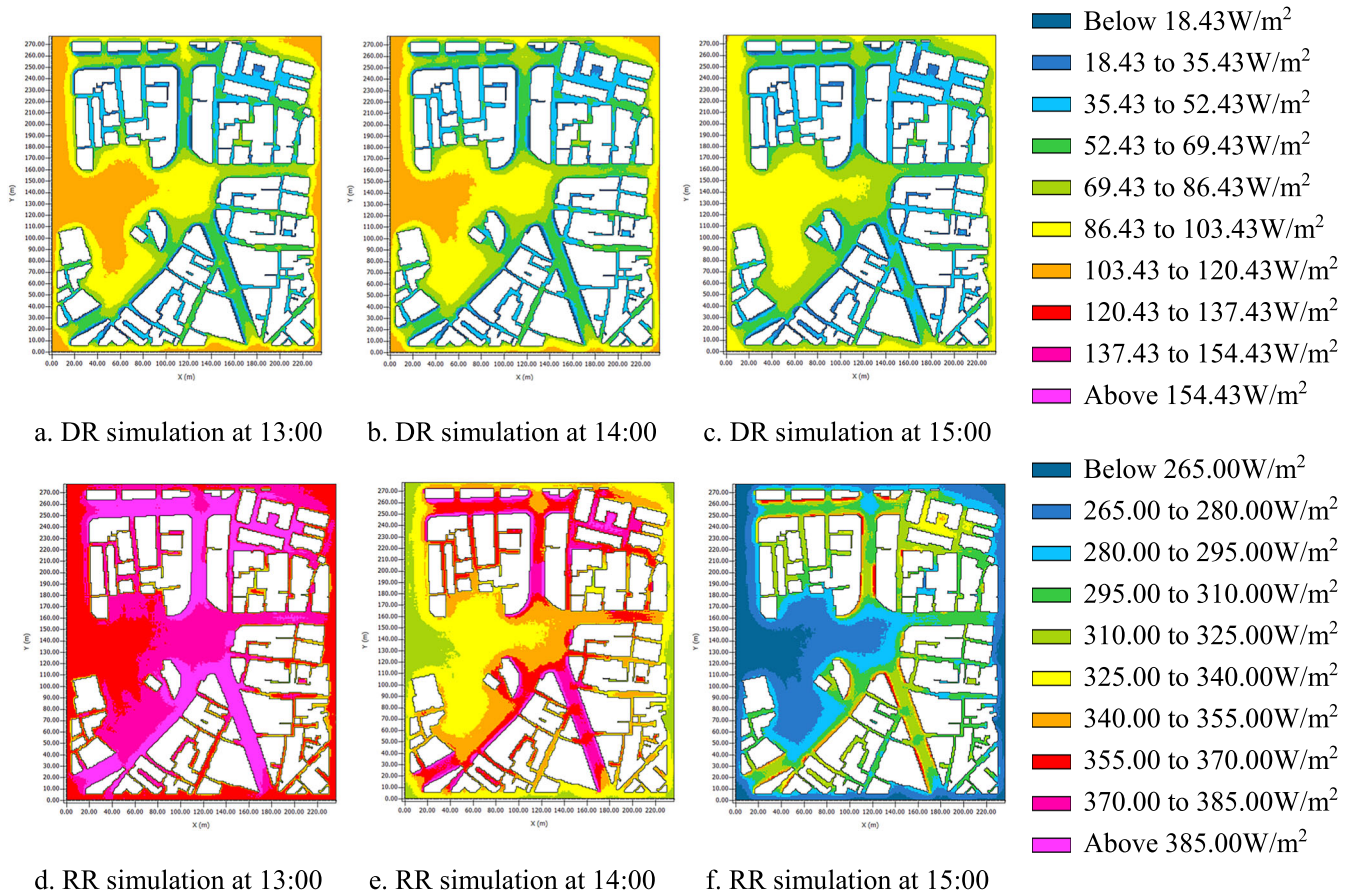
a. DR simulation at 13:00   b. DR simulation at 14:00   c. DR simulation at 15:00

d. RR simulation at 13:00   e. RR simulation at 14:00   f. RR simulation at 15:00

Fig. 8 | Simulated of DR and RR from 13:00 to 15:00. a DR simulation at 13:00; **b** DR simulation at 14:00; **c** DR simulation at 15:00; **d** RR simulation at 13:00; **e** RR simulation at 14:00; **f** RR simulation at 15:00. DR diffuse radiation, RR reflected radiation.
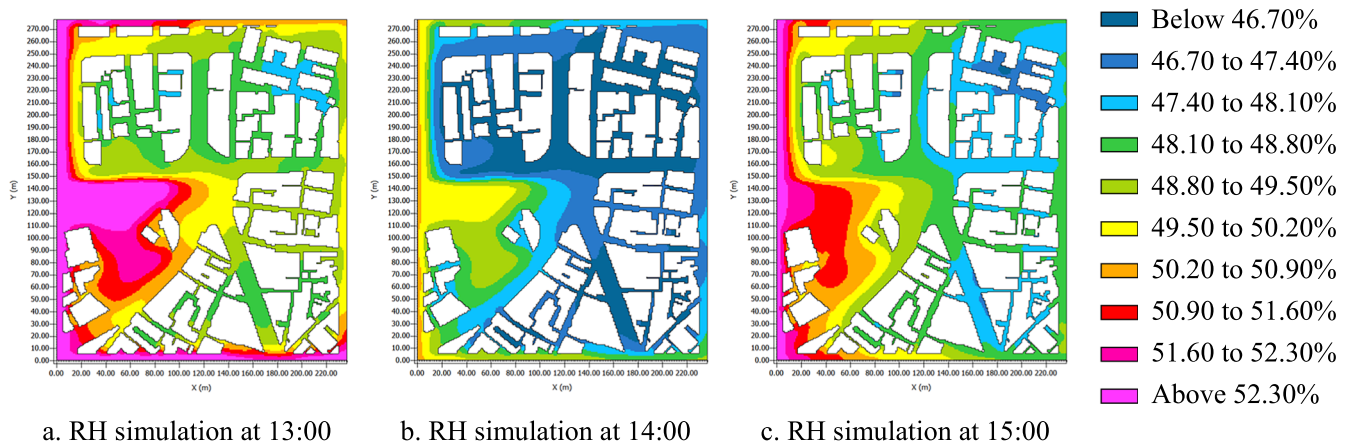

a. RH simulation at 13:00   b. RH simulation at 14:00   c. RH simulation at 15:00

Fig. 9 | Simulation of relative humidity distribution from 13:00 to 15:00. a RH simulation at 13:00; **b** RH simulation at 14:00; **c** RH simulation at 15:00. RH relative humidity.

tree arrangement. This layout also promotes local natural ventilation, allowing trees to fully utilize their transpiration effects and SR blocking capabilities.

The morphological and dimensional parameters of tree models, particularly the tree crown, are closely related to the results of urban thermal environment simulations[54–56]. As shown in Fig. 14, during the daytime heat periods in summer, the morphology of trees determines the position and size of tree shade, thereby producing different microclimate. The umbrella-shaped tree crown has a large shade area and high branching points,

resulting in excellent shading effects, minimal wind obstruction, and optimal cooling and humidifying effects. The spherical tree crown is less effective, while the tower-shaped tree crown has the smallest effective shaded area and lower branching points, causing more significant obstruction to air circulation. Considering the actual height of surrounding buildings, the greening plan selects umbrella-shaped tree crown trees with a height of 7 m and a crown spread of 5 m.

Scheme 1 has a tree coverage percentage of 25%; Scheme 2 has 50%; and Scheme 3 has 75%. All three schemes use the same tree species, which
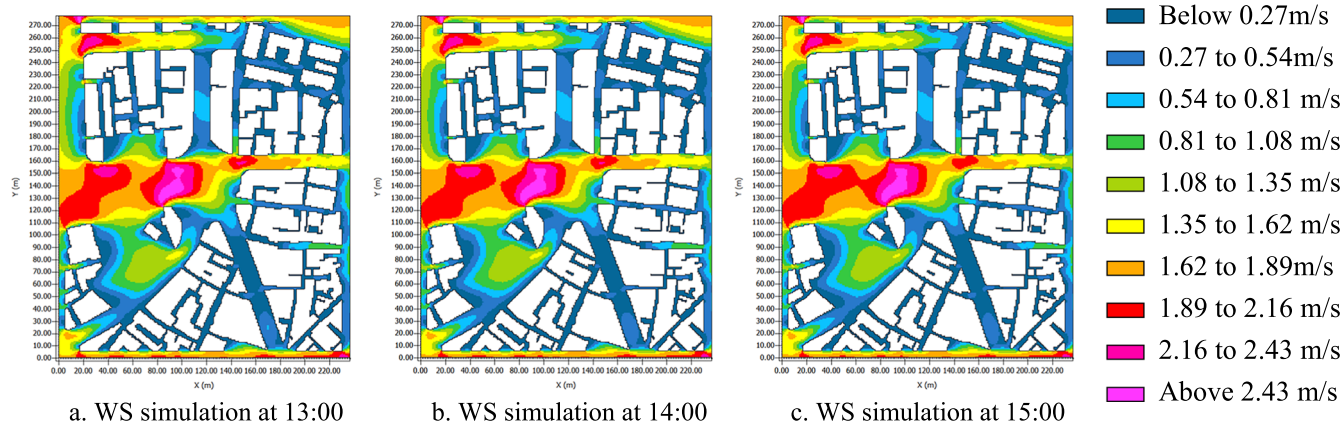
a. WS simulation at 13:00   b. WS simulation at 14:00   c. WS simulation at 15:00

Fig. 10 | Simulation of WS distribution from 13:00 to 15:00. a WS simulation at 13:00. **b** WS simulation at 14:00. **c** WS simulation at 15:00. WS wind speed.
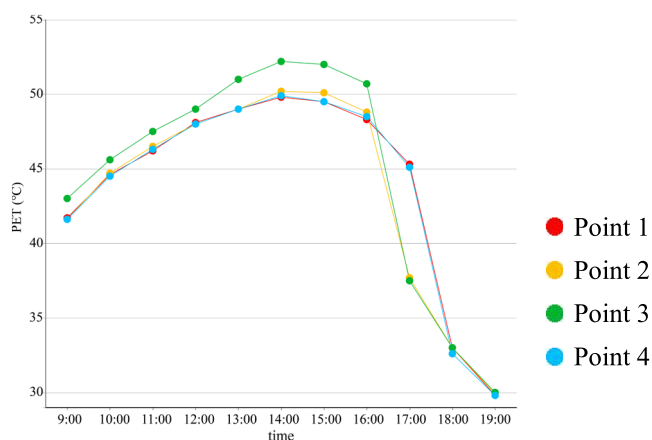

Fig. 11 | Hourly PET thermal comfort simulation values of measuring points 1–4. Red circle indicates point 1; Orange circle indicates point 2; Green circle indicates point 3; Blue circle indicates point 4. PET physiological equivalent temperature.

are planted in walking and resting areas, which helps provide effective shade for visitors. The paving materials are all low-luminance, light-colored permeable bricks, reducing absorption of SR. In terms of visual impact, trees are planted along the west side of Shengping Road to block the visual impact of the parking lot on the site entrance. Additionally, trees are planted next to the isolated historical building on the west side of the square to weaken the background visual impact when visitors view the historical building. Based on the three greening schemes, an ENVI-met model is established, with the initial meteorological parameters of the model being the same as those of the current simulation, and visualization of microclimate indices is conducted at a height of 1.5 m.

As shown in Figs. 15 and 16, we have selected the areas within the dashed-line boxes as specific evaluation zones. Compared to the original site without landscaping, the planting of trees and their shaded areas have significantly improved thermal comfort during the 14:00 and 15:00 time slots. In Scheme 1, which features a 25% tree coverage rate, approximately 27% of the area experienced a decrease in PET values ranging from 0.63 to 5.96 °C at 14:00, and about 33% of the area saw a reduction of 0.40 to 7.74 °C at 15:00. At the northeast entrance square, PET values increased by 0.4 to 0.6 °C at 14:00, but remained unchanged at 15:00. This phenomenon can be attributed to the change in paving material from soil to permeable pavement, as WS showed no significant variation during this period, as indicated by the previous microclimate analysis.

In Scheme 2, with a 50% tree coverage rate, approximately 53% of the area experienced a decrease in PET values ranging from 0.75 to 6.72 °C at 14:00, and about 64% of the area saw a reduction of 0.92 to 9.83 °C at 15:00.

At the northeast entrance square, PET values increased by 0.4 to 0.6 °C at 14:00, with minimal changes at 15:00. This was due to the combined effects of tree obstruction to ventilation on the west side of the site and the change in paving material from soil to permeable pavement. Additionally, this plan also improved thermal comfort in the external street spaces. At 14:00, approximately 10% of the area along the northern section of Guoping Road saw a decrease in PET values ranging from 0.31 to 0.57 °C, and about 2.5% of the area along the southeast section experienced a reduction of 0.45 to 0.83 °C. At 15:00, approximately 12.5% of the northern section saw a decrease of 0.49 to 1.87 °C, and about 12% of the southeast section experienced a reduction of 0.71 to 1.18 °C. The eastern section of Shengping Road saw a 25% area with PET values decreasing by 0.20 °C at both 14:00 and 15:00. Anping Road saw a decrease of 0.26 to 0.74 °C in approximately 2.5% of its area at both 14:00 and 15:00. Yuanqian Road only showed a decrease of 0.20 °C in about 10% of its area at 15:00.

In Scheme 3 with 75% tree coverage, at 14:00, approximately 78% of the area experienced a decrease in PET values ranging from 0.45 to 7.62 °C, and at 15:00, about 85% of the area exhibited a decrease in PET values ranging from 0.75 to 11.10 °C. The area with PET values exceeding 54.20 °C was significantly reduced compared with the original site. Additionally, this scheme had a notable impact on improving the external street spaces: at 14:00, about 17% of the area along the northern section of Guoping Road showed a decrease in PET values ranging from 0.36 to 1.31 °C, and about 4% of the area along the southeastern section demonstrated a decrease ranging from 0.48 to 0.97 °C. At 15:00, about 30% of the northern section and 14% of the southeastern section experienced decreases ranging from 0.65 to 2.28 °C and 0.76 to 1.46 °C. Along the eastern section of Shengping Road, 45% of the area had a PET decrease of 0.20 °C at both 14:00 and 15:00. Anping Road had a PET decrease of 0.20 to 1.37 °C in 5% of its area, and Yuanqian Road had a PET decrease of 0.20 to 0.40 °C in about 13% of its area, both at these times.

Although the association between urban green spaces and cooling effects is increasingly clear[57–59], the relationship between greenery and human thermal comfort remains worthy of discussion[60,61]. Comparing the optimization results of the three greenery design schemes, it is evident that during peak summer heat periods, Scheme 3 with 75% tree coverage provides the largest improvement in comfort, the greatest decrease in PET values, and the most significant impact on adjacent pedestrian streets. Scheme 2 with 50% tree coverage follows, while Scheme 1 with 25% tree coverage shows weaker improvements in thermal comfort. The optimization areas for Scheme 1 are mainly concentrated within the green-covered site, whereas Schemes 2 and 3 show a noticeable expansion of optimization areas, enhancing thermal comfort in nearby areas due to the introduction of greenery. This indicates that increasing greenery enhances the "Cool Island Spillover Effect"(CISE). However, this does not mean that higher tree coverage is always better, as in Schemes 2 and 3, certain areas experienced an
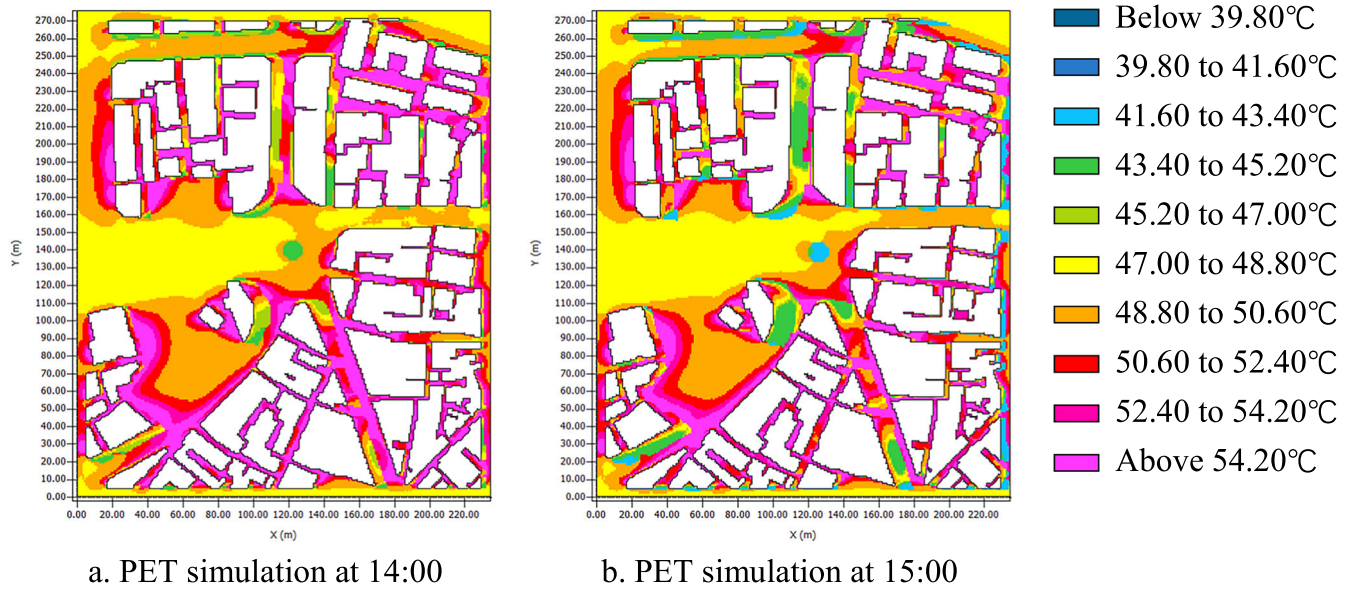
a. PET simulation at 14:00   b. PET simulation at 15:00

Fig. 12 | Simulation of PET distribution at 14:00 and 15:00. a PET simulation at 14:00; **b** PET simulation at 15:00. PET physiological equivalent temperature.
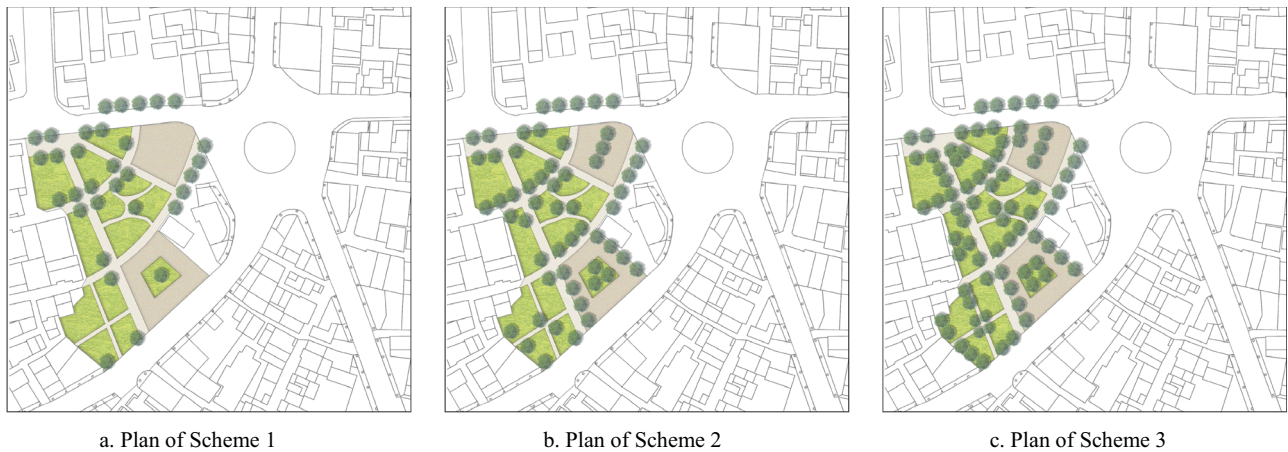

a. Plan of Scheme 1   b. Plan of Scheme 2   c. Plan of Scheme 3

Fig. 13 | Plans of three greening layout. a Plan of Scheme 1; **b** Plan of Scheme 2; **c** Plan of Scheme 3.

effective shaded area   effective shaded area   effective shaded area
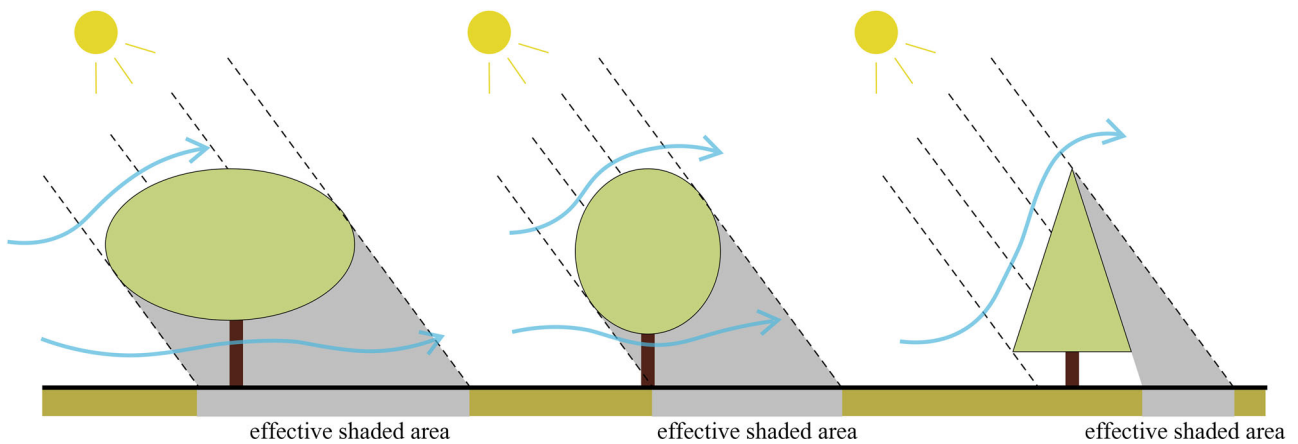
Fig. 14 | The effect of different trees on thermal environment of surrounding area.

increase in PET values of 0.87 to 1.67 °C due to the negative impact of high-density tree cover on ventilation and heat dissipation in those areas, suggesting that an appropriate tree coverage and strategic placement are more conducive to improving outdoor thermal comfort.

Regarding street spaces. As shown in Fig. 17, in most streets within the study area, the first-floor spaces along the streets recess inward to form public spaces for pedestrians, known as arcades. Most historical buildings have facades spanning 4-5 floors, and visitors can only fully view the facades
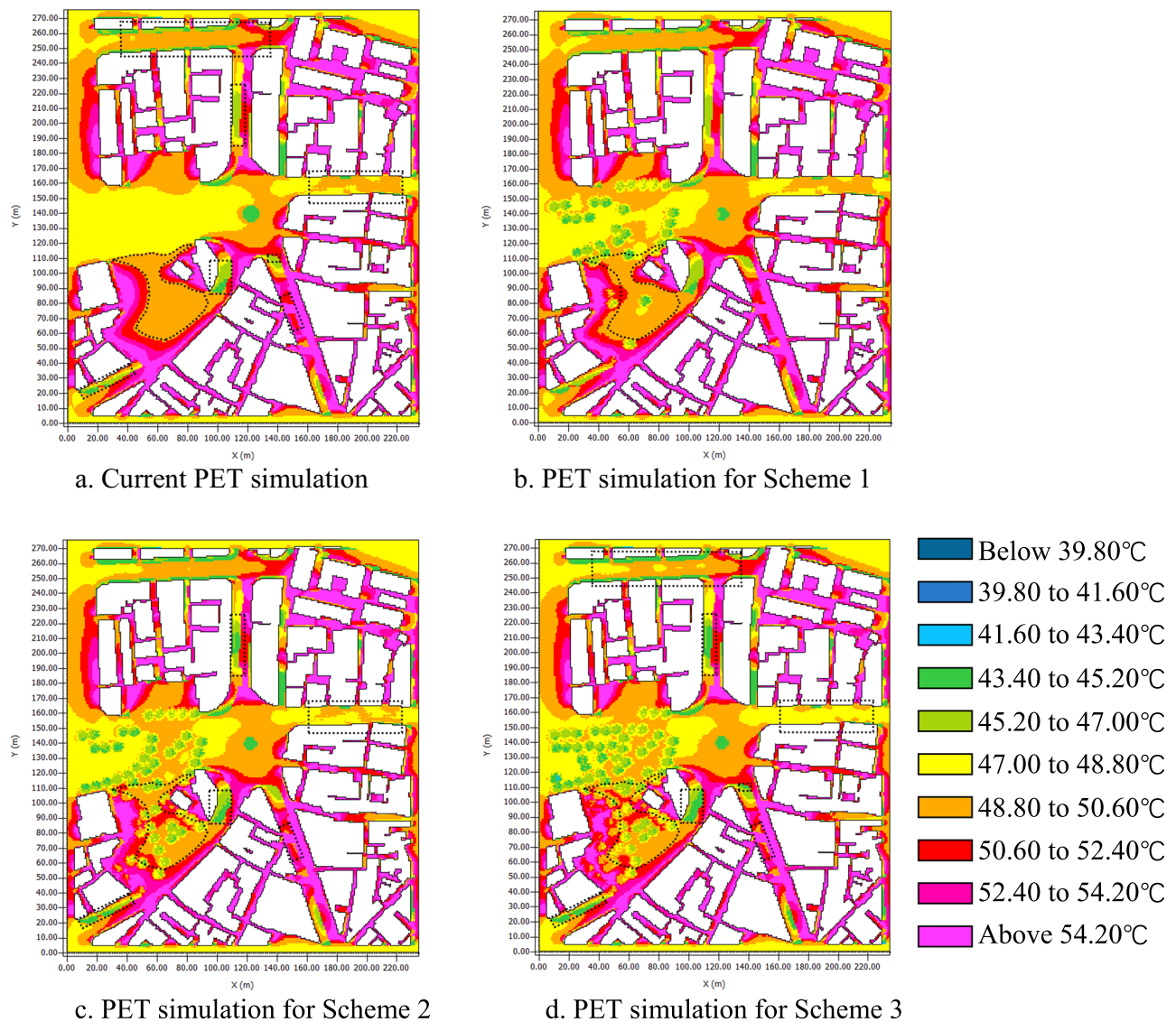
a. Current PET simulation

b. PET simulation for Scheme 1

c. PET simulation for Scheme 2

d. PET simulation for Scheme 3

Legend:
- Below 39.80℃
- 39.80 to 41.60℃
- 41.60 to 43.40℃
- 43.40 to 45.20℃
- 45.20 to 47.00℃
- 47.00 to 48.80℃
- 48.80 to 50.60℃
- 50.60 to 52.40℃
- 52.40 to 54.20℃
- Above 54.20℃

Fig. 15 | PET Simulation of Scheme 1–3 at 14:00. a Current PET simulation; **b** PET simulation for Scheme 1; **c** PET simulation for Scheme 2; **d** PET simulation for Scheme 3. The black dashed line represents the data analysis area. PET physiological equivalent temperature.

of each floor from corridors or streets if their line of sight is not obstructed. Based on visual analysis, under the constraint that the sightlines of visitors with a height of 1.7 m are not obstructed, plant heights should not exceed 2 m. The width of the pedestrian streets is approximately 10 m, and a 4-m-wide fire lane must be reserved on each side. Therefore, the width of street greening should also not exceed 2 m, making it suitable to adopt a greening approach combining shrubs with groundcovers.

As shown in Fig. 18, linear greening is added to the street space. Scheme 4 employs 1-meter-high shrubs combined with groundcovers, while Scheme 5 utilizes 2-meter-high shrubs combined with groundcovers. Apart from the difference in shrub height, the planting methods and paving materials are identical in both schemes. The green space ratio for each street is 10%. The initial meteorological parameters for the models are the same as those used in the previous microclimate status simulation, and visualizations of PET values are conducted at a height of 1.5 m.

As shown in Figs. 19 and 20, at 14:00 and 15:00, the PET simulation results of two linear greening schemes (Schemes 4 and 5) at a height of 1.5 m are compared with the current non-greening thermal simulation results, with the comparison scope indicated by the dashed line in the figure.

For the eastern section of Shengping Road, in Scheme 4, at 14:00, approximately 40% of the area surrounding the greenery experienced a PET

value decrease of 0.20–0.40 °C, and at 15:00, approximately 8% of the area showed a similar decrease. In Scheme 5, at 14:00, approximately 37% of the surrounding area had a PET value decrease of 0.20–0.40 °C, and at 15:00, approximately 10% of the area showed a similar decrease.

For the northern section of Guoping Road, in Scheme 4, at 14:00, approximately 3% of the area surrounding the greenery had a PET value decrease of 0.15–0.20°C, and at 15:00, about 10% of the area experienced a significant PET value decrease of 1.42–1.79 °C. In Scheme 5, at 14:00, approximately 21% of the surrounding area had a PET value decrease of 0.32–0.76 °C; at 15:00, about 14% of the area showed a PET value decrease of 1.55–2.11 °C. For the southeastern section of Guoping Road, in Scheme 4, at 14:00, there was no significant improvement in the PET values surrounding the greenery, while at 15:00, almost 6% of the area showed a PET value decrease of 0.96–1.48 °C; In Scheme 5, at 14:00, about 8% of the surrounding area had a PET value decrease of 0.63–1.55 °C, and at 15:00, about 20% of the area experienced a PET value decrease of 0.98–1.61 °C.

For Anping Road, according to Scheme 4, at 14:00, the PET values in approximately 4% of the area surrounding the greenery decreased by 0.20–0.53 °C; at 15:00, the PET values in approximately 6% of the surrounding green areas decreased by 0.20–2.73 °C. In Scheme 5, at 14:00, the PET values in almost 11% of the surrounding green areas decreased by
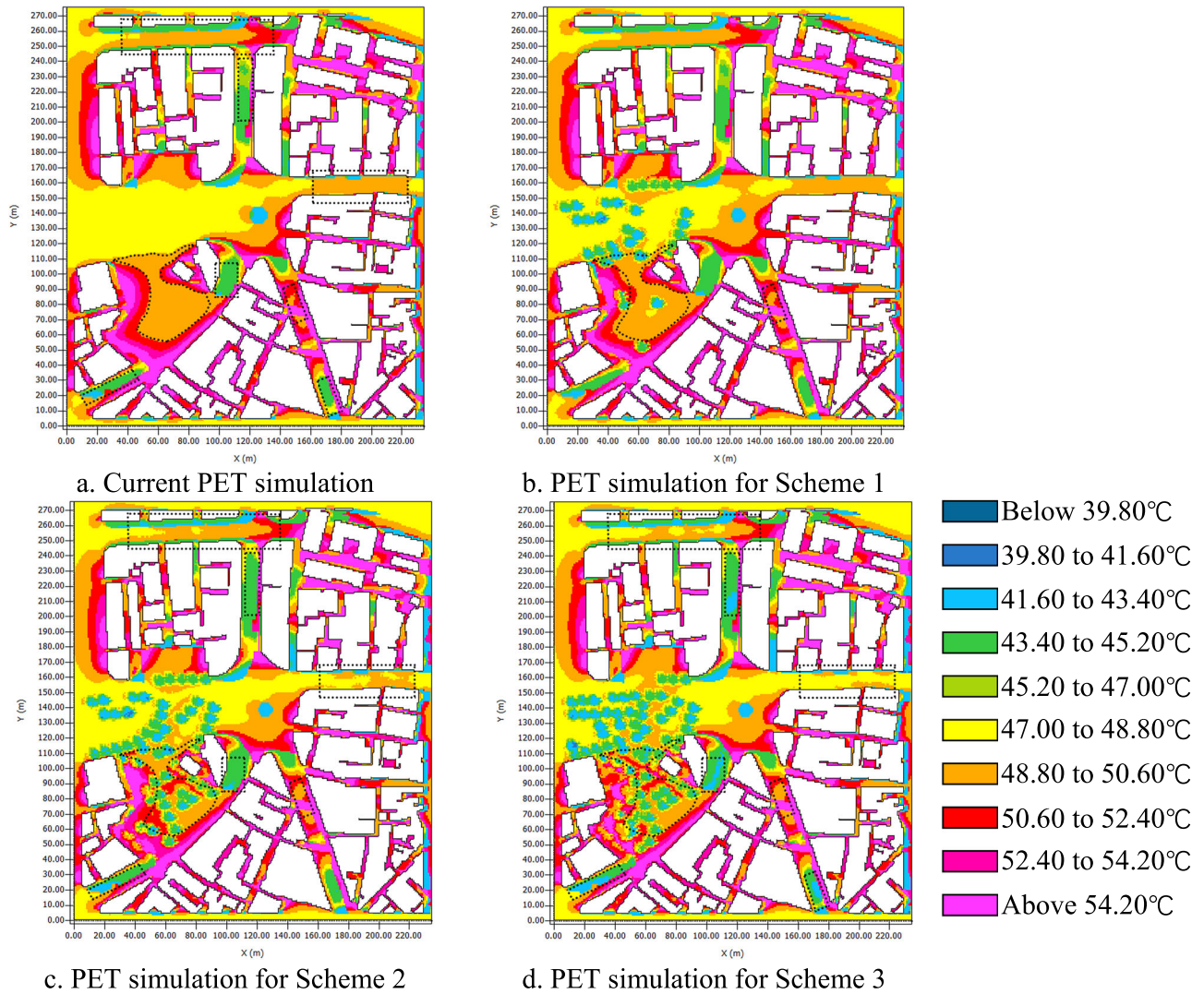
a. Current PET simulation   b. PET simulation for Scheme 1

c. PET simulation for Scheme 2   d. PET simulation for Scheme 3

Below 39.80℃
39.80 to 41.60℃
41.60 to 43.40℃
43.40 to 45.20℃
45.20 to 47.00℃
47.00 to 48.80℃
48.80 to 50.60℃
50.60 to 52.40℃
52.40 to 54.20℃
Above 54.20℃

Fig. 16 | PET Simulation of Schemes 1–3 at 15:00. a Current PET simulation; **b** PET simulation for Scheme 1; **c** PET simulation for Scheme 2; **d** PET simulation for Scheme 3. The black dashed line represents the data analysis area. PET physiological equivalent temperature.
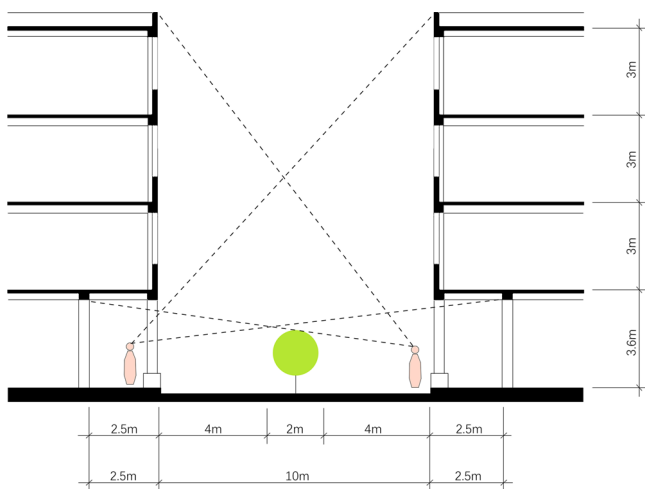
Fig. 17 | Analysis of street sightline. This figure shows the section of the street in the study. The black dashed line represents a person's sightline.

0.20–0.53 ℃; at 15:00, the PET values in about 13% of the surrounding green areas decreased by 0.17–3.73℃.

For Yuanqian Road, according to Scheme 4, at 14:00, the PET values in approximately 10% of the surrounding green areas decreased by 0.20–0.40 ℃; at 15:00, the PET values in about 8% of the surrounding green areas decreased by 0.20–0.40 ℃. In Scheme 5, at 14:00, the PET values in about 11% of the surrounding green areas decreased by 0.20 –0.40 ℃; at 15:00, the PET values in almost 10% of the surrounding green areas decreased by 0.20–0.40 ℃.

In summary, by comparing the PET optimization degree of the various streets, it can be seen that the improvement degree of Scheme 5 is generally superior to that of Scheme 4. Without obstructing visitors' sightlines, the use of taller shrubs can improve thermal comfort in more surrounding areas. However, compared to tree-based greening schemes, the areas improved by shrub-based greening remain relatively limited.

An optimized greening scheme suitable for high-density historical districts
As shown in Table 4, according to the thermal comfort improvement results of the 5 greening schemes: In the tree greening scheme with an area-based layout, the thermal comfort of Scheme 3 with 75% tree coverage is the best. During the hottest period of summer, from 14:00 to 15:00, the PET values within the observation range decreased by 0.45–11.10 ℃, with an average

optimized area ratio of 81.5%, forming a significant "Cool Island Effect" (CIE), which significantly reduced the PET values in the tree canopy coverage area, helping to quickly improve the thermal comfort of aggregated crowds. Combined with the conclusions from Section 3.1, this greening scheme also reduced the PET values of the surrounding street spaces by 0.20–2.88 °C, with the improved area ratio reaching up to 45%. A high-coverage tree greening scheme can also produce a more pronounced "Cool Island Spillover Effect" (CISE), benefiting pedestrians dispersed in the surrounding spaces. In the two shrub greening schemes with linear layouts, Scheme 5 (2 m-tall shrubs) has 50% more green volume than Scheme 4 (1 m-tall shrubs), calculated based on the same planting density and average canopy width. Simulation results show that Scheme 5 has better thermal comfort, with PET values within the observation range decreasing by 0.20–3.73 °C, an average optimized area ratio of 14.5%, and the optimized area concentrated within 1 meter around the green belt. The CISE is insufficient, failing to affect more distant district spaces, and only prioritizes the improvement of thermal comfort for pedestrians near the green belt.

Overall, under the same indicators, such as plant configuration principle and site conditions, area-based greening is more effective in improving the overall thermal environment, significantly reducing the PET values in the greening coverage area. However, it is important to avoid excessive tree coverage leading to poor local heat dissipation. Additionally, due to site area constraints, it is difficult to add large area-based greening in high-density historical districts. The introduction of linear greening, although unable to significantly lower PET values, has stronger targeting for pedestrian thermal comfort optimization and can be flexibly arranged in the middle or on both sides of the streets, making it more suitable for flexible and dispersed placement in high-density historical districts.

As shown in Table 5, to compare the cost-effectiveness of the five schemes and help planners quantify the "greening investment— thermal comfort benefit" relationship, we further define the cooling efficiency of greening using "the decrease in PET (°C per 1% greening rate) and the ratio of thermal comfort improvement area per 1% greening rate," with the calculation formulas as follows:

$$E_T = \frac{T_{avg}}{G} \tag{1}$$

Note: E_T represents the temperature improvement efficiency (°C/1% green coverage); T_{avg} is the mean value of the PET reduction range (°C); G represents the green coverage rate (%).

$$E_A = \frac{A_r}{G} \tag{2}$$

Note: E_A represents the area improvement ratio (ratio/1% greening rate); A_r represents the proportion of the improved thermal comfort area to the observed area (%); G represents the greening rate (in %).

From the calculation results in the table, it can be seen that the temperature improvement efficiency (ET) of the patchy tree greening scheme exhibits diminishing unit benefits as the greening rate increases (with the cooling efficiency per 1% greening rate decreasing under high coverage). The ET at 14:00 decreases from 0.26 to 0.11 for -Schemes 1 to 3, while the area improvement ratio (EA) remains stable at 0.0104–0.0108, indicating that the cool island spillover effect can drive a comprehensive improvement in thermal comfort across the entire observation area. In the linear shrub scheme, the 1 m tall shrubs (Scheme 4) have a higher temperature improvement efficiency (0.29 at both 14:00 and 15:00) due to their proximity to pedestrian height and minimal obstruction to ventilation. Meanwhile, the EA at 14:00 for the 2 m tall shrubs (Scheme 5) is 0.0170, the highest in the entire table, demonstrating the local efficiency of low-level
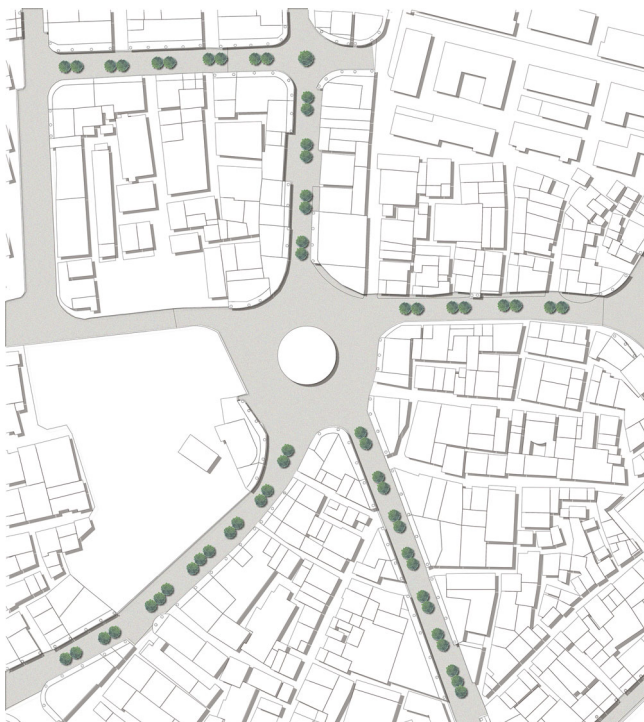

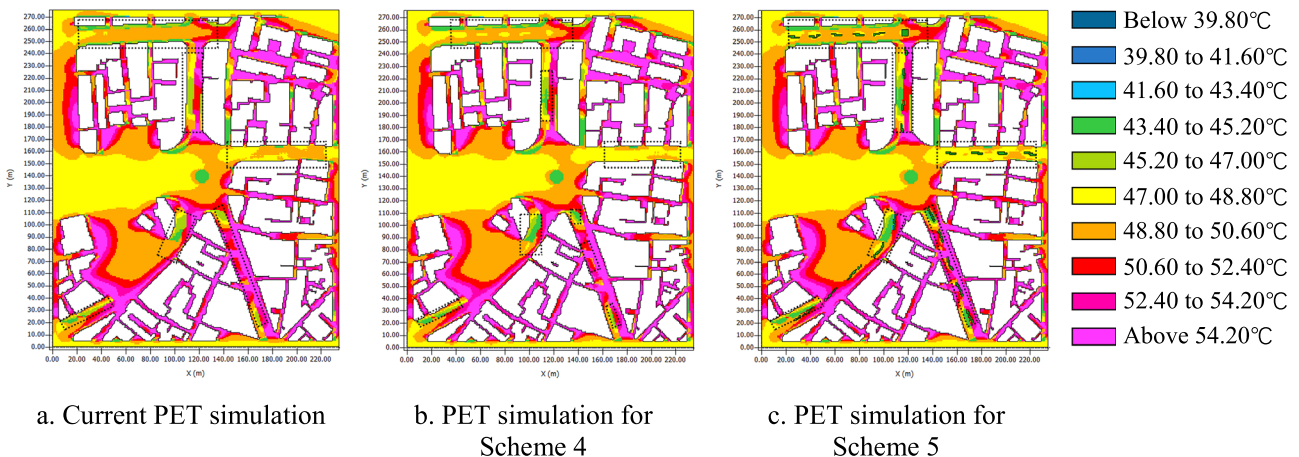**Fig. 18 | Layout plan of linear greening.**

a. Current PET simulation

b. PET simulation for Scheme 4

c. PET simulation for Scheme 5

■	Below 39.80℃
■	39.80 to 41.60℃
■	41.60 to 43.40℃
■	43.40 to 45.20℃
■	45.20 to 47.00℃
■	47.00 to 48.80℃
■	48.80 to 50.60℃
■	50.60 to 52.40℃
■	52.40 to 54.20℃
■	Above 54.20℃

Fig. 19 | PET simulation of Schemes 4 and 5 at 14:00. a Current PET simulation; **b** PET simulation for Scheme 4; **c** PET simulation for Scheme 5. The black dashed line represents the data analysis area. PET physiological equivalent temperature.
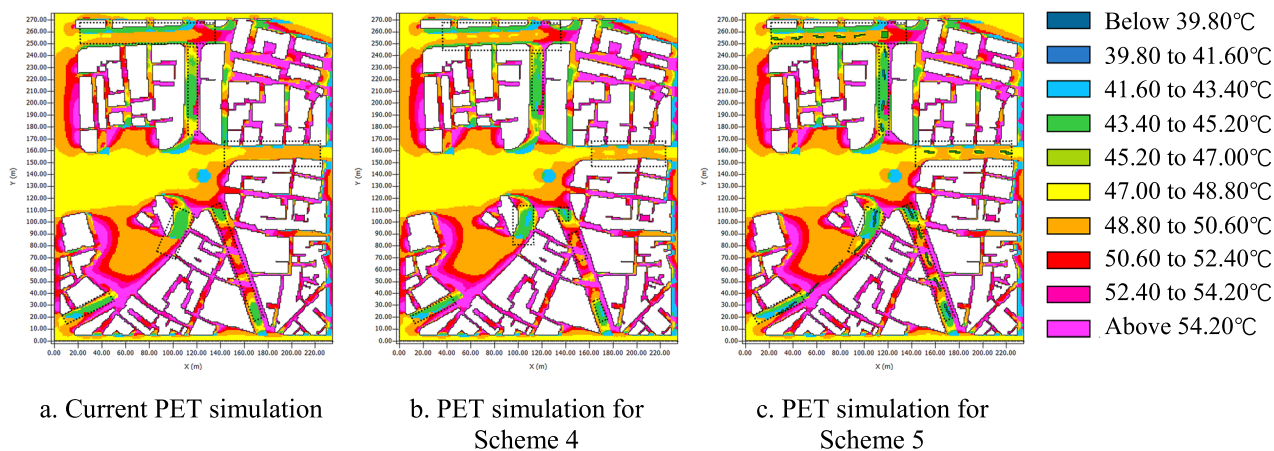
a. Current PET simulation | b. PET simulation for Scheme 4 | c. PET simulation for Scheme 5

Fig. 20 | PET simulation of Schemes 4 and 5 at 15:00. a Current PET simulation; **b** PET simulation for Scheme 4; **c** PET simulation for Scheme 5. The black dashed line represents the data analysis area. PET physiological equivalent temperature.

Table 4 | Impact of 5 greening schemes on thermal comfort

Greening plan		Greening type	Tree coverage rate	Plant height, crown diameter (m)	Improvement at 14:00 Cooling range (°C)/Area ratio (%)	Improvement at 15:00 Cooling range (°C)/Area ratio (%)
Area-based greening	Schemes1	Tree, vegetation	25%	7*5	0.63–5.96, 27%	0.40–7.47, 33%
	Schemes2	Tree, vegetation	50%	7*5	0.75–6.72, 53%	0.92–9.83, 64%
	Schemes3	Tree, vegetation	75%	7*5	0.45–7.62, 78%	0.75–1 1.10,85%
Linear greening	Schemes4	Shrubs	10%	1*2	0.15–2.73, 13%	0.20–2.73, 8%
	Schemes5	Shrubs	10%	2*2	0.20–1.55, 17%	0.17–3.73, 12%

Note: 1. The temperature reduction range includes the difference between the shaded and non-shaded areas of trees. 2. The area ratio is based on ENVI-met grid counting.

Table 5 | Comparison of greening investment and thermal comfort benefits

Greening plan	greening rate	14:00		15:00	
		E_T (°C/1% green coverage)	E_A (ratio/1% greening rate)	E_T (°C/1% green coverage)	E_A (ratio/1% greening rate)
Scheme1	25%	0.26	0.0108	0.32	0.0132
Scheme2	50%	0.15	0.0106	0.22	0.0116
Scheme3	75%	0.11	0.0104	0.16	0.0113
Scheme4	10%	0.29	0.0130	0.29	0.0080
Scheme5	10%	0.18	0.0170	0.39	0.0012

shading. Overall, the patchy scheme with a 50% greening rate (Scheme 2) strikes a balance between cooling efficiency and coverage, making it suitable for comprehensive optimization of open spaces. Linear greening, on the other hand, is more suitable for localized enhancement in narrow streets, with 1 m tall shrubs emphasizing a balance between ventilation and shading, and 2 m tall shrubs focusing on precise cooling in vertical spaces. The above data provides a quantitative basis for the "form-efficiency" relationship in greening planning for high-density historic districts, namely selecting greening forms based on spatial scale and functional needs: preferring patchy trees with a coverage rate of 50–75% in open areas to leverage their spillover effect for overall thermal environment improvement; and opting for intermittent linear shrubs 1–2 m tall in narrow streets to achieve a synergy of "comprehensive cooling and localized enhancement".

In similar research cases, historical districts exhibit three prominent characteristics: high building density, high pedestrian density, and a high proportion of "very hot" areas. These constraints necessitate that efforts to enhance outdoor thermal comfort through increased greenery must simultaneously address the protection of heritage buildings, the coordination of building facades, the width of fire lanes, and unobstructed visitor views. This imposes detailed requirements on the form and scale of

greenery. Different spaces within historical districts, such as squares, vacant lots, main streets, alleys, and areas around heritage buildings, require tailored greenery strategies. Beyond the trees and shrubs mentioned in the simulation plans, a more diverse range of greenery types can enhance the targeting and adaptability of greenery schemes. For instance, movable greenery and vertical greenery can increase layout flexibility, shallow-rooted greenery can minimize damage to heritage building foundations, and native plants can strengthen the environmental adaptability of greenery plans. As shown in Table 6, we present a greenery strategy matrix that illustrates the correspondence between different spatial types and greenery types in Shantou port districts, along with key design considerations.

In addition to selecting a reasonable greenery strategy, adhering to the design process is equally crucial. During the current thermal comfort assessment phase, priority levels for greenery implementation are determined based on the thermal comfort grades of different areas. Areas with a PET greater than 50.6 °C (such as the west side of the central square) are classified as the first priority, areas with a PET between 45.2 and 50.6 °C are the second priority, and areas with a PET between 39.8 and 45.2 °C are the third priority. In the preliminary design phase of the greenery plan, following the "minimum intervention" principle, greenery strategies are

Table 6 | Greening strategy matrix of the study area

| Area	Space features	Greening	Key points of design
Square, vacant land	1. Open space (H/D < 0.5) 2. Tourist gathering areas, high density, long stay duration.	Area-based greening	1. Umbrella-shaped trees ($H = 7$ m, coverage rate 50–75%); 2. Linear layout; 3. Permeable pavement with low reflectivity. 4. Unobstructed area at the entrance and exit with width of 4 m.
Main street	1. Radial pattern around the central square, with width of ≥10 m and H/D ratio of 0.8–1.5. 2. The width of the fire escape lane on each side is ≥4 m.	Linear greening.	1. A 2 m-high shrub belt arranged along the arcade colonnade; 2. Movable potted plants added in between. 3. The width of the shrub belt is ≤2 m, and the spacing between potted plants is ≥6 m.
Branch streets and alleys	1. The road width is ≥5 m, and H/D ≥ 2. 2. The width of the fire escape lane is ≥4 m.	Vertical greening	1. Wall climbing plants, wall planting bags, and hanging plants suspended from eaves. 2. Avoid ground trees and plants.
Surrounding areas of buildings	The area within a 1-m= radius around the heritage buildings is a no-planting zone.	Shallow- rooted greening	1. Shallow-rooted herbaceous plants planted in flower box. 2. The planting area shall not be adjacent to the external wall.
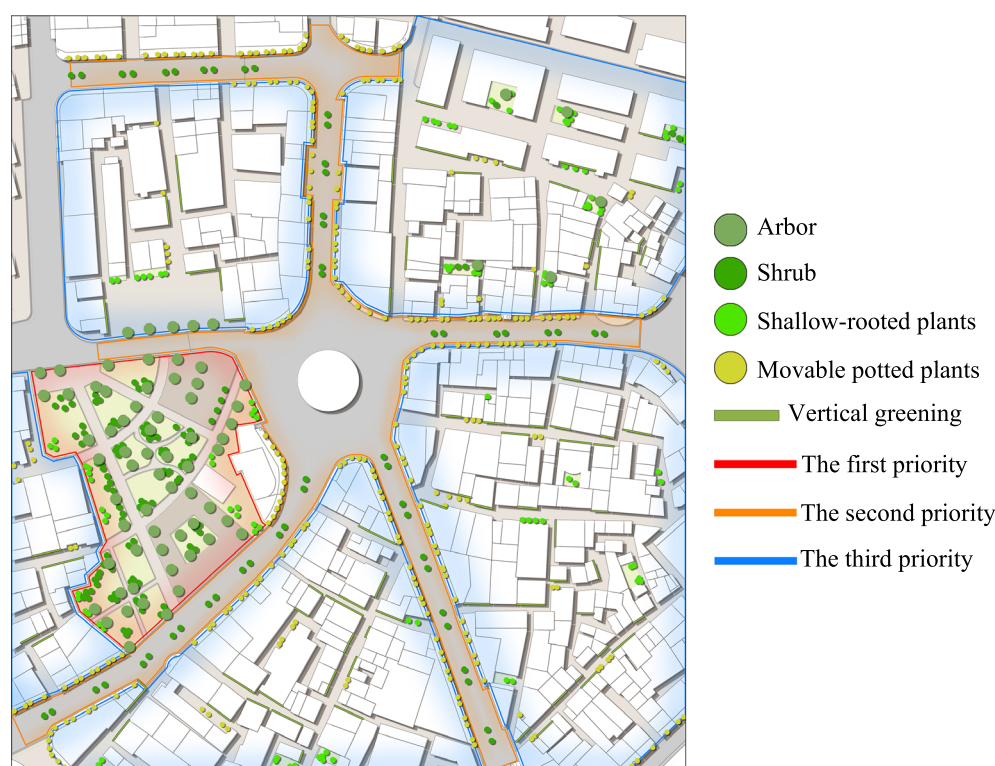
Fig. 21 | The greenery distribution plan of the study area. Green circle indicates plants; Green line indicates vertical greenery; Red line indicates the first priority; Orange line indicates the second priority; Blue line indicates the third priority.

allocated to various areas based on the greenery strategy matrix of Table 6, with different greenery rates such as 10%, 25%, 50%, and 75% configured to form multiple greenery plans. During the thermal comfort simulation calculation phase, the simulated PET results of each plan are compared with the current non-greening thermal environment to quantify the extent and area of thermal comfort improvement, and the correlation between greenery plans and the district's pedestrian thermal comfort is analyzed with reference to Tables 4 and 5. Specifically, Table 4 provides basic data such as the cooling range and improved area ratio of each scheme, while Table 5 offers quantitative indicators like temperature improvement efficiency (ET) and area improvement ratio (EA), which together support the correlation analysis. In the optimization design phase, the impact characteristics of greenery forms, greenery rates, and plant scales on the study area are evaluated, providing a basis for the formulation of optimized greenery plans.

As shown in Fig. 21, following the above four design processes, we have designed the greenery distribution plan for the historical district of Shantou City.

Discussion

Under the international consensus on the conservation of built heritage, urban morphological characteristics in high-density historical districts are protected by heritage regulations[62,63]. However, within the context of rapid urbanization, many such districts, including the "port-opening area" of Shantou city, have experienced overdevelopment for commercial purposes, resulting in a notable lack of greening that exacerbates urban heat stress[6,7]. This issue is compounded by studies showing that insufficient greenery coverage significantly contributes to resident dissatisfaction with outdoor thermal environments in historical areas[16], while the cooling potential of

vegetation is often constrained by high-density urban morphology that limits solar exposure for many green spaces[64]. This paper addresses the widespread issue of degraded thermal comfort by examining the impact of different outdoor greening configurations. Focusing on two types of potential greening sites, arcaded streets and vacant land, we propose five greening design schemes to systematically evaluate how greening form and volume influence PET. Building upon previous studies that highlight the role of vegetation in microclimate regulation[15,60], this research aims to enhance the efficiency and accuracy of greening design in heritage-sensitive urban environments, offering a approach to balancing thermal comfort with preservation needs.

Our findings echo existing knowledge that vegetation plays a crucial role in microclimate regulation, and further refine this principle through quantitative analysis. The demonstrated cooling effects of greening align with broader consensus in the field, yet our study advances this knowledge by differentiating the microclimate impacts of area-based versus linear greening configurations, as well as tree versus shrub plantings (Table 4). This distinction resonates with research showing that different planting patterns and species combinations yield varying cooling benefits[65], and that trees generally provide superior cooling effects compared to grass surfaces[19]. The observed "Cool Island Spillover Effect" (CISE) from the 75% tree canopy coverage scheme (Scheme 3) underscores the district-scale potential of concentrated greening in open spaces. This phenomenon, while recognized in broader urban green space studies[57,58], is specifically quantified here for the constrained context of a historic district, echoing findings that large, contiguous green spaces produce more pronounced cooling effects[64]. Conversely, the targeted improvements from linear shrub schemes (Schemes 4 & 5) highlight the necessity of context-specific solutions, resonating with research emphasizing the need for tailored approaches in complex urban fabrics[53] and studies demonstrating that optimizing tree arrangement according to solar exposure significantly enhances cooling efficiency[29]. A core contribution of this work lies in introducing cost-effectiveness metrics (ET and EA), offering a new perspective for planners. Unlike studies focusing primarily on alternative strategies like high-reflectance materials[9] or shading facilities[10], our research quantifies the "form-efficiency" relationship of greening itself. The data revealing higher immediate cooling efficiency for 1 m shrubs but greater area improvement ratio for 2 m shrubs (Table 5) provides a basis for decision-making, helping to balance "ventilation-priority" versus "local-cooling-priority" needs in different street contexts. However, the study also reveals complexities. The slight PET increase in certain areas of Schemes 2 and 3, attributed to impeded ventilation, serves as a critical reminder that greening design must holistically consider air movement alongside SR, a challenge also noted in studies of high-density urban greenery[66]. This insight reinforces the value of a diversified greening toolkit, as proposed in our strategy matrix (Table 6), which suggests adaptable solutions like movable planters and vertical greening for varied micro-spaces, consistent with research advocating for multidimensional greening approaches in space-constrained historical districts[21] and studies demonstrating the thermal benefits of vertical greening systems in high-density environments[27].

It is important to note the specific context in which this study's findings are situated. The quantitative outcomes and the proposed greening strategy matrix (Table 6) are primarily applicable to high-density historic districts in southern coastal cities of China, characterized by a hot-humid subtropical climate and a built fabric dominated by arcade buildings. The strategy of prioritizing cooling, selecting plants such as umbrella-shaped trees, and addressing specific constraints including a 2 m height limit for shrubs to preserve heritage sightlines and a 4 m fire lane reservation, are direct responses to this unique context. Consequently, these specific strategies may not be directly transferable to historic districts in other climatic zones, such as temperate regions where solar access in winter is a key concern, or to districts with different architectural heritage typologies and conservation regulations.

Under the constraints of international heritage conservation, the distinctive morphology of high-density historic districts is both a cultural asset and a source of thermal discomfort. This study navigates the critical challenge of improving livability without altering the protected urban fabric. It advances strategic greening as a viable path forward, and through a comparative analysis of design option supported by field data and simulation, proposes a data-driven methodology for deploying greening strategies with precision and efficacy. The main conclusions are as follows:

First, the spatial distribution of thermal comfort is highly heterogeneous, dictated by the interplay of street morphology and SR. The period between 14:00 and 15:00 was identified as the most critical, with PET values exceeding 43 °C across the study area, categorizing the thermal sensation as "very hot." Areas with insufficient shading, such as sections of Anping Road, and spaces with constrained ventilation, like the southern part of Guoping Road, were identified as priority zones for intervention.

Second, the efficacy of greening is highly dependent on its configuration. For open spaces, patchy greening with trees is paramount. The 75% canopy coverage scheme achieved the most significant cooling, reducing PET by 0.45–11.10 °C for 85% of the area and generating a valuable "Cool Island Spillover Effect" that improved adjacent streets. However, diminishing returns in cooling efficiency at higher coverage rates suggest an optimal range of 50–75%, which balances maximum benefit with resource investment. For constrained street canyons, where trees are impractical, linear greening with 1–2 m high shrubs provides targeted relief, reducing PET by 0.17–3.73 °C without obstructing heritage sightlines or fire lanes.

Third, the core innovation of this research lies in its methodology. The introduction of cost-effectiveness metrics (ET and EA) quantifies the "greening investment-thermal comfort benefit" relationship, providing urban planners with a tangible decision-support tool. The proposed greening strategy matrix further translates these findings into actionable design guidelines tailored to specific spatial types within historic districts.

In conclusion, while the specific greening configurations and design strategies proposed in this study are tailored to the context of Shantou's port-opening area, the methodological framework established here holds broader relevance. The integrated approach of field measurement, targeted greening scheme design, and ENVI-met simulation provides a replicable model for thermal comfort optimization in other high-density historic districts, particularly within similar subtropical climates. Furthermore, the introduction of cost-effectiveness metrics (E_T and E_A) offers a versatile tool for evaluating the efficiency of different greening interventions. Nevertheless, this study acknowledges certain limitations, primarily its focus on a single typical summer day and a consistent set of plant parameters. Future research should incorporate longitudinal studies across seasons, explore a wider variety of plant species with differentiated physiological traits, and integrate social surveys to assess perceived comfort. Finally, the synergistic effects of combining strategic greening with other passive cooling strategies warrant further investigation.

Data availability

References

1. Wu, B. H., Liu, L., Shao, J. & Morrison, A. M. The evolution and space patterns of hutongtels in Beijing historic districts. *J. Herit. Tour.* **10**, 129–150 (2015).
2. Huang, N., Cai, Y. J., Zhuang, M. Y., Zhou, Y. & Zhou, J. Spatial regeneration for preservation of historic urban features and improvement of living conditions in high-density historic districts: urban renewal design strategies for Shanghai's old town. *Int. J. High Rise Build.* **10**, 9–16 (2021).
3. Fang, K. L. & Wu, Y. F. The importance of integrating historic context and activities into heritage district: enhancing attraction and vitality. *npj Herit. Sci.* **13**, 434 (2025).

4. Battista, G., Carnielo, E. & Vollaro, R. D. L. Thermal impact of a redeveloped area on localized urban microclimate: a case study in Rome. *Energy Build.* **133**, 446–454 (2016).

5. Li, N., Guo, Z., Geng, W. Y., Li, L. & Li, Z. W. Design strategies for renovation of public space in Beijing's traditional communities based on measured microclimate and thermal comfort. *Sustain. Cities Soc.* **99**, 104927 (2023).

6. Liu, W. Q., Miao, C., Xiao, L., Mai, J. H. & Wang, Y. Z. Layout optimization of residential buildings to improve the outdoor microclimate of neighborhoods along an urban bay: a case study of Shantou's Inner Bay, China. *Buildings* **14**, 3912 (2024).

7. Zheng, B. H., Bedra, K. B., Zheng, J. & Wang, G. G. Combination of tree configuration with street configuration for thermal comfort optimization under extreme summer conditions in the urban center of Shantou City, China. *Sustainability* **10**, 4192 (2018).

8. Ye, Z. Q., Song, S. & Zhong, R. F. Temporal and spatial evolution of climate comfort and population exposure in Guangdong Province in the last half century. *Atmosphere* **13**, 502 (2022).

9. Huang, J. P. *Report on the development of the Shantou Special Economic Zone in Annual Report on the Development of China's Special Economic Zones (2018) Blue Book of China's Special Economic Zones* (eds Tao, Y. & Yuan, Y.) 131–140 (Springer Singapore, 2019).

10. Tao, H., Wen, J. M., Zhu, H. & Zhang, Q. Analysis of spatial mismatch of tourism development in Guangdong province. *J. Resour. Ecol.* **9**, 181–190 (2018).

11. Deng, G. & Chen, H. H. The spatiotemporal characteristics and driving factors of regional ecological efficiency in the tourism sector. *Sustainability* **16**, 982 (2024).

12. Jamei, E. & Ossen, D. R. Intra urban air temperature distributions in historic urban center. *Am. J. Environ. Sci.* **8**, 503–509 (2012).

13. Chu, Y. C., Hsu, M. F. & Hsieh, C. M. A field assessment on natural ventilation and thermal comfort of historical district-a case of the Wugoushui Settlement in Taiwan. *J. Sci. Eng. Res.* **5**, 463–472 (2015).

14. Ragheb, A. A., El-Darwish, I. I. & Ahmed, S. Microclimate and human comfort considerations in planning a historic urban quarter. *Int. J. Sustain. Built Environ.* **5**, 156–157 (2016).

15. Castaldo, V. L., Pisello, A. L., Pigliautile, I., Piselli, C. & Cotana, F. Microclimate and air quality investigation in historic hilly urban areas: experimental and numerical investigation in central Italy. *Sustain. Cities Soc.* **33**, 27–44 (2017).

16. Biqaraz, B., Fayaz, R. & Naeeni, G. H. A comparison of outdoor thermal comfort in historical and contemporary urban fabrics of Lar City. *Urban Clim.* **27**, 212–226 (2019).

17. Bochenek, A. D. & Klemm, K. Effectiveness of tree pattern in street canyons on thermal conditions and human comfort. Assessment of an urban renewal project in historical district in Lodz (Poland). *Atmosphere* **12**, 751 (2021).

18. Yang, X., Li, S. T., Zhang, Q. & He, S. Thermal comfort assessment of the Beijing Historical Town Blocks: analysis of indices and applications. *Sci. Program.* **2022**, 1–18 (2022).

19. Ng, E., Chen, L., Wang, Y. N. & Yuan, C. A study on the cooling effects of greening in a high-density city: An experience from Hong Kong. *Build. Environ.* **47**, 256–271 (2012).

20. Qi, L., Li, T., Chang, B. Y. & Xiong, W. Research on thermal comfort evaluation and optimization of green space in Beijing Dashilar Historic District. *Buildings* **14**, 3121 (2024).

21. Jim, C. Y. Trees and high-density urban development: opportunities out of constraints. *Habitat Int* **17**, 13–29 (1993).

22. Rosso, F. et al. On the impact of innovative materials on outdoor thermal comfort of pedestrians in historical urban canyons. *Renew. Energy* **118**, 825–839 (2018).

23. Yildirim, M. Shading in the outdoor environments of climate-friendly hot and dry historical streets: the passageways of Sanliurfa, Turkey. *Environ. Impact Assess. Rev.* **80**, 106318 (2020).

24. Sui, Q., Jia, H., Zhao, M., Zhou, Y. & Fan, L. Quantitative evaluation of ecosystem services of urban street trees: A case study of Shengjing Historical and cultural block in Shenyang, China. *Sustainability* **15**, 2532 (2023).

25. Li, Y. N. et al. Assessing thermal comfort for the elderly in historical districts and proposing adaptive urban design strategies: a case study in Zhenjiang, China. *Landsc. Ecol. Eng.* **21**, 29–46 (2025).

26. Ma, D. X., Wang, Y. P., Zhou, D., Zhu, Z. Z. & Yang, Y. J. The renew plans of urban thermal environment optimization for traditional districts in Xi'an, China. *Environ. Sci. Pollut. Res.* **30**, 5700–5716 (2022).

27. Morakinyo, T. E., Lai, A., Lau, K. K.-L. & Ng, E. Thermal benefits of vertical greening in a high-density city: Case study of Hong Kong. *Urban For. Urban Green.* **37**, 42–55 (2019).

28. Ge, J. J. et al. Cooling energy saving by vegetation planting in high-density districts: Evaluation using the coupled simulation. *Build. Environ.* **232**, 110054 (2023).

29. Wu, Z. F. & Chen, L. D. Optimizing the spatial arrangement of trees in residential neighborhoods for better cooling effects: integrating modeling with in-situ measurements. *Landsc. Urban Plan.* **167**, 463–472 (2017).

30. Yang, Y. J. Planning method of centralized greening in high-rise residential blocks based on improvement of thermal comfort in summer. *Sustain. Cities Soc.* **80**, 103802 (2022).

31. Enescu, D. A review of thermal comfort models and indicators for indoor environments. *Renew. Sustain. Energy Rev.* **79**, 1353–1379 (2017).

32. Zhang, J. L., Li, Z. & Hu, D. Effects of urban morphology on thermal comfort at the micro-scale. *Sustain. Cities Soc.* **86**, 104150 (2022).

33. Sansaniwal, S. K., Mathur, J. & Mathur, S. Review of practices for human thermal comfort in buildings: present and future perspectives. *Int. J. Ambient Energy* **43**, 1–67 (2020).

34. Deb, C. & Alur, R. Review of studies on outdoor thermal comfort using physiological equivalent temperature (PET). *J. Inst. Eng. India Archit. Eng. Div.* **92**, 38–41 (2011).

35. Nikolopoulou, M. & Lykoudis, S. Thermal comfort in outdoor urban spaces: analysis across different European countries. *Build. Environ.* **41**, 1455–1470 (2006).

36. Villadiego, K. & Velay-Dabat, M. A. Outdoor thermal comfort in a hot and humid climate of Colombia: a field study in Barranquilla. *Build. Environ.* **75**, 142–152 (2014).

37. Knez, I., Thorsson, S., Eliasson, I. & Lindberg, F. Psychological mechanisms in outdoor place and weather assessment: towards a conceptual model. *Int. J. Biometeorol.* **53**, 101–111 (2009).

38. Algeciras, J. A. R., Consuegra, L. G. & Matzarakis, A. Spatial-temporal study on the effects of urban street configurations on human thermal comfort in the world heritage city of Camagüey-Cuba. *Build. Environ.* **101**, 81–85 (2016).

39. Liu, J. Y., Tang, H. F. & Zheng, B. H. Simulation study of summer microclimate in street space of historic conservation areas in China: A case study in Changsha. *Front. Environ. Sci.* **11**, 1146801 (2023).

40. Lee, J. H. & Ham, Y. Physiological sensing-driven personal thermal comfort modelling in consideration of human activity variations. *Build. Res. Inf.* **49**, 1–13 (2020).

41. Potchter, O., Cohen, P., Lin, T.-P. & Matzarakis, A. Outdoor human thermal perception in various climates: a comprehensive review of approaches, methods and quantification. *Sci. Total Environ.* **631**, 390–406 (2018).

42. Yau, Y. H., Toh, H. S., Chew, B. T. & Nik Ghazali, N. N. A review of human thermal comfort model in predicting human–environment interaction in non-uniform environmental conditions. *J. Therm. Anal. Calorim.* **147**, 1–25 (2022).

43. Kang, G. & Kim, J. J. How to plant trees on an elevated road to improve thermal comfort in a street canyon. *Sustain. Cities Soc.* **121**, 106207 (2025).

44. Wu, S. B., Yu, W. B. & Chen, B. Observed inequality in thermal comfort exposure and its multifaceted associations with greenspace in United States cities. *Landsc. Urban Plan.* **233**, 104701 (2023).

45. Cheng, Y. Y. et al. Thermal comfort analysis and optimization strategies of green spaces in Chinese traditional settlements. *Forests* **14**, 1501 (2023).

46. Gál, T., Lindberg, F. & Unger, J. Computing continuous sky view factors using 3D urban raster and vector databases: comparison and application to urban climate. *Theor. Appl. Climatol.* **95**, 111–123 (2009).

47. Lin, L. Q., Deng, Y. Y., Peng, M., Zhen, L. X. & Qin, S. W. Multi-scale influence analysis of urban shadow and spatial form features on urban thermal environment. *Remote Sens* **15**, 4902 (2023).

48. Osman, A. H., Artus, M., Alsaad, H., Koch, C. & Voelker, C. Assessing thermoelectric radiative cooling partition as a personalised comfort system using empirical experiments enhanced by digital shadow visualisation. *Build. Environ.* **245**, 110833 (2023).

49. Lindberg, F. & Grimmond, C. S. B. The influence of vegetation and building morphology on shadow patterns and mean radiant temperatures in urban areas: Model development and evaluation. *Theor. Appl. Climatol.* **105**, 311–323 (2011).

50. Lin, T. P. & Matzarakis, A. Tourism climate and thermal comfort in Sun Moon Lake, Taiwan. *Int. J. Biometeorol.* **52**, 281–290 (2008).

51. Cheng, V., Ng, E., Chan, C. & Givoni, B. Outdoor thermal comfort in sub-tropical climate: A longitudinal study based in Hong Kong. *Int. J. Biometeorol.* **56**, 43–56 (2011).

52. Li, K. M., Zhang, Y. F. & Zhao, L. H. Outdoor thermal comfort and activities in the urban residential community in a humid subtropical area of China. *Energy Build* **133**, 498–511 (2016).

53. Lin, T. P. Thermal perception, adaptation and attendance in a public square in hot and humid regions. *Build. Environ.* **44**, 2017–2026 (2009).

54. Buccolieri, R., Santiago, J.-L., Rivas, E. & Sanchez, B. Review on urban tree modelling in CFD simulations: aerodynamic, deposition and thermal effects. *Urban For. Urban Green.* **31**, 212–220 (2018).

55. Zeng, F. X., Lei, C. W., Liu, J. L., Niu, J. L. & Gao, N. P. CFD simulation of the drag effect of urban trees: source term modification method revisited at the tree scale. *Sustain. Cities Soc.* **56**, 102079 (2020).

56. Li, R. B. et al. CFD simulations of the tree effect on the outdoor microclimate by coupling the canopy energy balance model. *Build. Environ.* **230**, 109995 (2023).

57. Zhang, Q., Zhou, D., Xu, D. & Rogora, A. Correlation between cooling effect of green space and surrounding urban spatial form: evidence from 36 urban green spaces. *Build. Environ.* **222**, 109375 (2022).

58. Sun, T., Chen, L. D. & Sun, R. H. Cooling effects in urban communities: Parsing green spaces and building shadows. *Urban For. Urban Green.* **94**, 128264 (2024).

59. Tan, X. Y., Sun, X., Huang, C. D., Yuan, Y. & Hou, D. L. Comparison of cooling effect between green space and water body. *Sustain. Cities Soc.* **67**, 102711 (2021).

60. Rui, L. Y., Buccolieri, R., Gao, Z., Gatto, E. & Ding, W. W. Study of the effect of green quantity and structure on thermal comfort and air quality in an urban-like residential district by ENVI-met modelling. *Build. Simul.* **12**, 1–12 (2018).

61. Xue, F., Gou, Z. H. & Lau, S. S. Y. Green open space in high-dense Asian cities: Site configurations, microclimates and users' perceptions. *Sustain. Cities Soc.* **34**, 114–125 (2017).

62. Gospodini, A. Urban morphology and place identity in European cities: built heritage and innovative design. *J. Urban Des.* **9**, 225–248 (2004).

63. Mosler, S. Everyday heritage concept as an approach to place-making process in the urban landscape. *J. Urban Des.* **24**, 778–793 (2019).

64. Shih, W. Y. Greenspace patterns and the mitigation of land surface temperature in Taipei metropolis. *Habitat Int.* **60**, 69–80 (2017).

65. Abdi, B., Hami, A. & Zarehaghi, D. Impact of small-scale tree planting patterns on outdoor cooling and thermal comfort. *Sustain. Cities Soc.* **56**, 102085 (2020).

66. Huang, J. X., Hao, T. P., Wang, Y. L. & Jones, P. A street-scale simulation model for the cooling performance of urban greenery: evidence from a high-density city. *Sustain. Cities Soc.* **82**, 103908 (2022).

Acknowledgements

Author contributions

L.W.Q. and W.Y.Z.: conceptualization, interpretation, and method analysis; Y.S., L.W.Q., and M.J.H.: data collection and quality, simulation and visualization; M.J.H and L.W.Q.: writing-review and editing; Y.S. and H.H.S.: editing the manuscript. All authors read and approved the final manuscript.

Competing interests

The authors declare no competing interests.

Additional information

Correspondence and requests for materials should be addressed to Wenqing Liu or Yingzi Wang.

Reprints and permissions information is available at
http://www.nature.com/reprints

Publisher's note Springer Nature remains neutral with regard to jurisdictional claims in published maps and institutional affiliations.